FINAL REPORT

Field Assessment of Abiotic Attenuation Rates using Chemical Reactivity Probes and Cryogenic Core Collection

SERDP Project ER-2621

AUGUST 2020

Richard L. Johnson, PI
Paul G. Tratnyek, Co-PI
Oregon Health & Science University

SERDP
DOD ▪ EPA ▪ DOE

REPORT DOCUMENTATION PAGE

Form Approved
OMB No. 0704-0188

1. REPORT DATE *(DD-MM-YYYY)*	**2. REPORT TYPE**	**3. DATES COVERED** *(From - To)*
25/08/2020	SERDP Final Report	9/7/2016 - 9/7/2021

4. TITLE AND SUBTITLE

Field Assessment of Abiotic Attenuation Rates using Chemical Reactivity Probes and Cryogenic Core Collection

5a. CONTRACT NUMBER
16-C-0044

5b. GRANT NUMBER

5c. PROGRAM ELEMENT NUMBER

6. AUTHOR(S)
Richard L. Johnson
Paul G. Tratnyek

5d. PROJECT NUMBER
ER-2621

5e. TASK NUMBER

5f. WORK UNIT NUMBER

7. PERFORMING ORGANIZATION NAME(S) AND ADDRESS(ES)
Oregon Health & Science University
3181 SW Sam Jackson Road HRC3
Portland, OR 97239

8. PERFORMING ORGANIZATION REPORT NUMBER
ER-2621

9. SPONSORING/MONITORING AGENCY NAME(S) AND ADDRESS(ES)
Strategic Environmental Research and Development Program (SERDP)
4800 Mark Center Drive, Suite 16F16
Alexandria, VA 22350-3605

10. SPONSOR/MONITOR'S ACRONYM(S)
SERDP

11. SPONSOR/MONITOR'S REPORT NUMBER(S)
ER-2621

12. DISTRIBUTION/AVAILABILITY STATEMENT
DISTRIBUTION STATEMENT A. Approved for public release: distribution unlimited.

13. SUPPLEMENTARY NOTES

14. ABSTRACT
The overarching goal of this project was to develop new tools for measuring, and ultimately predicting, in situ abiotic reduction rates of groundwater contaminants of concern (CoCs). The approach to accomplish this was to collect well-preserved field cores using the cryogenic core collection technique and then test those cores in the laboratory to assess abiotic reduction rates.

15. SUBJECT TERMS
Abiotic Natural Attenuation, Reduction Potential, Reduction Rate, Cryogenic Core Collection, Groundwater Remediation, Chlorinated Hydrocarbons

16. SECURITY CLASSIFICATION OF:			**17. LIMITATION OF ABSTRACT**	**18. NUMBER OF PAGES**	**19a. NAME OF RESPONSIBLE PERSON**
a. REPORT	**b. ABSTRACT**	**c. THIS PAGE**			Richard L. Johnson
UNCLASS	UNCLASS	UNCLASS	UNCLASS	88	**19b. TELEPHONE NUMBER** *(Include area code)* 503-860-5957

Table of Contents

Table of Figures

Table of Tables

Acronyms

ANA	Abiotic Natural Attenuation
AVS	Acid-volatile sulfides
C^3	cryogenic core collection
CF	chloroform (trichloromethane)
CFE	chlorofluoroethene
CH4	methane
CM	chloromethane
CO	carbon monoxide
CO2	carbon dioxide
CoC	contaminant of concern
CS2	carbon disulfide
CT	carbon tetrachloride
DCE	dichloroethene
DCFE	dichlorofluoroethene
DCM	dichloromethane
DG	down gradient
DoD	Department of Defense
E	reduction potential
E_{ES}	electron shuttle mediated reduction potential
EZVI	emulsified zero valent iron
FE	fluoroethene
Fe(OH)2	ferrous hydroxide
Fe(II)/Fe^{2+}	ferrous iron
FeS	iron sulfide
FEW	F.W. Warren Air Force Base
GC	gas chromatograph
GC/ECD	gas chromatograph/electron capture detector
GC/MS/FID	gas chromatograph/mass spectrometer/flame ionization detector
HCOO	formate
I4S	indigo tetrosulfonate
IH	Indian Head, MD
kCF	CT →CF rate constant
kCO	CT→CO rate constant
kCS2	CT→CS2 rate constant
kCT	CT degradation rate constant
kHCOO	CT→HCOO rate constant

kM	mass-normalized rate constant
Kobs	observed rate constant
kUNK	CO → UNK rate constant
M	soil to water ratio
OU	operational unit
PI	Parris Island, SC
Redox	oxidation/reduction
RMI	reactive mineral intermediate
RP	reactivity probe
Rsf	resorufin
RTR	rolling tube reactor
Rzn	resazurin
S^{2-}	sulfide ion
SA	surface area
SHE	Standard hydrogen electrode
SLOP	St. Louis Ordinance Plant
SSA_R	Specific reactive surface area
TCE	trichloroethene
TCFE	trichlorofluoroethene
TCP	1,2,3-trichloropropane
ZVI	zero-valent iron

Keywords

Abiotic Natural Attenuation

Reduction Potential

Reduction Rate

Cryogenic Core Collection

Groundwater Remediation

Chlorinated Hydrocarbons

Acknowledgements

We would like to acknowledge the support of SERDP staff and contractors and our scientific colleagues, who helped us implement changes in project tasks as our collective understanding of abiotic reactions evolved over the last few years. We would also like to thank those involved in field sample collection. In particular, Rick Rogers and his team at Drilling Engineers, Dr. Tom Sale and crew from Colorado State, Dr. Mitch Olson and colleagues from Tryhydro, Inc., and Dr. Tim Mattes from Iowa State.

.

Abstract

The overarching goal of this project was to develop new tools for measuring, and ultimately predicting, *in situ* abiotic reduction rates of groundwater contaminants of concern (CoCs). The approach to accomplish this was to collect well-preserved field cores using the cryogenic core collection technique and then test those cores in the laboratory to assess abiotic reduction rates.

Two independent but complimentary measurement approaches were used. The first involves a reactivity probe, in this case carbon tetrachloride (CT), to measure abiotic reduction rates in batch experiments. The second involves careful measurement of reduction potential (*E*) using a platinum electrode and electron shuttle molecules that facilitate electrical contact between the electrode and the surfaces of aquifer solids in slurried samples. The reactivity and reduction potential measurement for each field sample were then plotted against each other to demonstrate a correlation that could be used to predict reaction rate. This approach is represented schematically in the figure below, where the photo on the right shows the "rolling tube reactors" used for the CT reactivity measurements and the photo on the left represents the process of measuring reduction potential using a combination electrode and an electron shuttle. As part of this work we also demonstrated that the predictive power of this approach can be somewhat enhanced by including pH in the correlation equation.

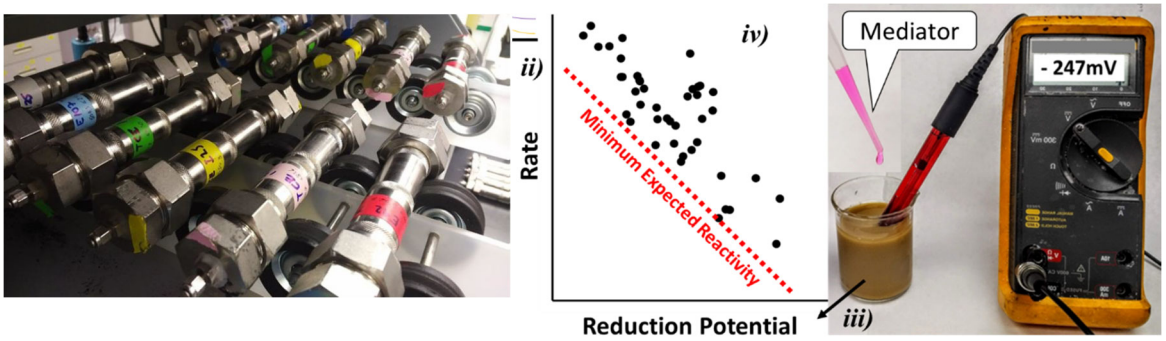

The processes of freezing and storage have the potential to alter the reactivity of the soils. To examine this, we used materials taken from laboratory columns operated under iron and sulfate reducing conditions and compared their reactivity after being frozen and stored for 60 days against samples that had never been frozen. The data showed, in general, that there was no significant loss of reactivity as the result of freezing and storage.

This project has resulted in an approach where core samples from field sites can be quickly assessed to determine the rate at which abiotic reduction is likely to occur in situ. This assessment can be accomplished either by direct measurement of reactivity in batch tests, or by careful measurement of reduction potential and the use of a correlation equation.

The next steps in the development of this approach should be: 1) its expanded use at field sites; 2) comparison to other methods for estimating abiotic reactivity; 3) expanding the range of reactivity probes to include other CoCs; and 4) characterization of the relationship between reduction products and the mineral phases that control their formation

1. Executive Summary

1.A. Introduction

Role of abiotic reduction in subsurface contaminant removal

Abiotic degradation of chlorinated solvents by reduced iron minerals is an important tool for addressing DoDs groundwater contamination challenges. The minerals responsible for abiotic natural attenuation (ANA) can be of natural (bio)geochemical origin or can be formed in situ as a result of active groundwater treatment. ANA reactions, although slow, can be significant over timeframes relevant for groundwater restoration (e.g., decades). However, such slow reaction rates are difficult to study in the laboratory, often requiring experiments over many months, and are even harder to measure in the field.

Recent evidence suggests that the active *in situ* formation of mineral phases is important for ANA. Formation of these minerals is likely to be highly dependent on the ferrous iron concentration, which in turn driven by dissimilatory iron reduction . Under those circumstances, these phases likely are continuously formed and consumed by biotic and abiotic geochemical processes, so we are calling them reactive mineral intermediates (RMIs). RMIs likely include very high surface area amorphous solid coatings, and/or colloids and nanoparticles. The study of these RMIs requires a paradigm shift in how the responsible phases are characterized, including approaches that preserve the reactivity of those phases to allow them to be examined in the laboratory. One of those approaches is cryogenic core collection, where the core sample is frozen *in situ* and delivered frozen to the laboratory. Evaluation of this approach for reactivity measurements was an important task in this project.

The relationship between reduction potential and reduction rate

In remediation practice, measurement of reduction potential (E) of well-water samples has been widely used as a proxy abiotic reactivity. However, conventional E measurements on water-only samples are not predictive of contaminant reduction rates in groundwater, mainly because they do not reflect potentials on the mineral surfaces where reactions occur (Shi et al., 2011). However, if a relationship between E and reaction rates could be established, it would be in important step forward in predicting ANA.

Stewart et al (2018) recently developed a correlation between rate of nitrobenzene reduction, pH, and reduction potential. Their general equation for this relationship was:

$$\log(k_{SA}) = \mathrm{a}\left(\frac{E}{0.059}\right) + b\ \mathrm{pH} + c \qquad [1.1]$$

Where k_{SA} is the surface-area normalized rate constant for a reaction, and *a, b*, and *c* are constants characteristic of that reaction.

For field samples composed of mixed mineralogy, reactive surface areas (SSA_R) cannot be measured, so we have transformed equation 1.1 into a mass-normalized version, where the term *c'* is a constant that also contains the unknown reactive surface area for the sample.

$$log(k_M) = a\left(\frac{E}{0.059}\right) + b\ \text{pH} + c + \log(SSA_R) \quad [1.2]$$

$$\log(k_M) = \text{a}\left(\frac{E}{0.059}\right) + b\ \text{pH} + c' \quad [1.3]$$

For a given field site, it may be reasonable to assume that the reactive surface area, SSA_R, and soil to water ratio (M, g L^{-1}) are relatively constant, and thus a linear relationship between E and log (k_M) might be expected. However, across a range of field sites it is expected that these values could vary significantly. Consequently, the hypothesis that Equation 1.3 is applicable across multiple field sites needs to be tested. To accomplish this, accurate measurements of both rate constants and reduction potentials would be required. As mentioned above, because the role of mineral surfaces is important, well-preserved field samples (e.g., cryogenic core collection) will be required for both of those measurements. Furthermore, accurate measurement of reduction potentials requires intimate contact between the measurement electrode and mineral surfaces. Electron shuttles (ESs) have emerged as one approach to improve reduction potential measurements of heterogeneous media. This study demonstrates the utility of high-quality ES-based reduction potential measurements and reactivity measurements using cryogenically-collected field cores to predict abiotic reduction rates.

1.B. Project Objectives

As discussed above, our understanding of the nature of reactive phases that are important for ANA has evolved significantly in the last few years. Indeed, even at the outset of this project (2016) it was generally believed that different mineral phases (e.g., magnetite, goethite, pyrite) had "intrinsic" surface-area-normalized reduction rates associated with them. As we have learned in the last few years, biological sources of dissolved ferrous iron can significantly enhance reactivity (e.g.,Culpepper 2018) As a result, while the objectives of the project have not changed, this evolution in understanding led to some significant shifts in the experiments conducted to accomplish project objectives. These are described briefly below.

Three objectives were identified in the original proposal for this work:

Objective 1. Demonstrate the utility of reactivity probes (RPs) over a broad range of geochemical conditions.

Objective 2. Evaluate the use of RPs to measure abiotic reaction rates of actual field samples collected with the cryogenic core method.

Objective 3. Integrate the data from the first two objectives to determine if one or more of the RPs can provide robust measures of contaminant degradation rates using cryogenically-collected core samples.

1.C. Technical Approach

Objective 1 – Demonstrate the utility of reactivity probes over a range of geochemical conditions

Our original proposal called for examination of reduction rates in batch experiments using a range of commercially-obtained mineral phases. However, based on experiments conducted in our lab and elsewhere, early in the project it became evident that reactivities of individual mineral phases could be dramatically altered under common geochemical conditions (e.g., iron- and sulfate-reducing environments.) As a consequence, we shifted from batch experiments to a pair of column experiments in which controlled biogeochemical conditions could be maintained under steady-state conditions (Figure 1.1)

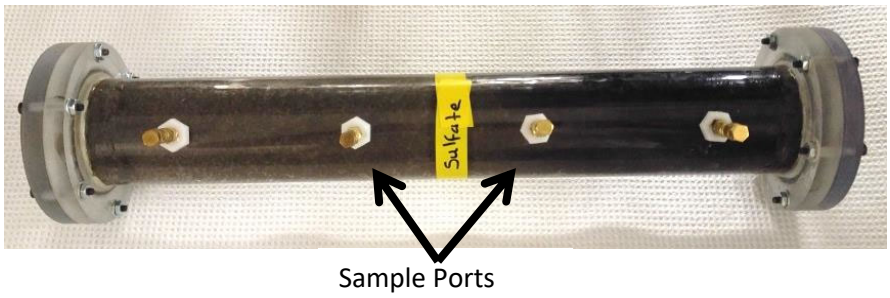

Figure 1.1. Laboratory column showing sampling ports. Sulfate was added to this column (S1) resulting in a transformation of solid phase color from gray to black that was not observed in the column without sulfate (M1).

In both cases, magnetite was added to the columns because it is widely believed to be effective for abioticly reducing chlorinated hydrocarbons and because it can serve as the source of biogenically-derived ferrous iron. Lactate was added as part of the bicarbonate-buffered, anoxic groundwater flowing through the column. For one column, sulfate was continuously added to the influent groundwater. The columns were operated until geochemical parameters (pH, ferrous iron, sulfate, sulfide) stabilized, and then reactivity probe experiments were initiated.

We began these experiments with a suite of reactivity probes, including redox-sensitive dyes (resazurin, indigo tetrasulfonate, indigo disulfonate), chlorinated contaminants (carbon tetrachloride – CT; trichloroethene – TCE; and a halogenated TCE analog trichlorofluoroethene - TCFE). Through a series of experiments we determined that the reaction rates of the dyes were too rapid to be useful for kinetics measurements, TCE was too slow (as will be discussed later) and our analog compound TCFE was not sufficiently stable in water. In contrast, CT had a number of characteristics that made it an ideal reactivity probe. These include: 1) well characterized reaction pathways, 2) first-order reaction rates that resulting in reaction times of a few days, 3) degrades primarily by abiotic pathways, and 4) not commonly present at most DoD sites.

As part of this task, CT and TCE were periodically injected (along with 1,2,3-trichloropropane as a conservative internal standard) into the column influents for a period of ~4 days to allow RP concentrations in the column to stabilize. The column residence time was ~0.5 days, and none of the compounds sorbed significantly, such that ~8 pore volumes had passed through the column during the injection period. At the conclusion of the injection process, column flow was stopped and the columns were intermittently sampled for parent compound, degradation products and internal standard.

Reaction rates were then determined for the disappearance of the parent compound as well as for each measured reaction product. Following each test, flow through the column was re-initiated without the chlorinated compounds for a period of several months to allow biogeochemical conditions to re-stabilize before subsequent tests.

Objective 2 - Measure abiotic reaction rates of actual field samples collected with the cryogenic core method.

A key goal of this project was to determine if the use of reactivity probes on high-quality soil cores would allow prediction of field reduction rates. Based on earlier SERDP work, we chose cryogenic core collection (C^3) as the means of collecting field cores. Our intent was to use the same reactivity probes for the field samples as were used for the columns in Objective 1. (Part of our strategy for evaluating the applicability of the C^3 plus RP approach was to use materials from the columns to evaluate how freezing and storage affected reactivity. This is discussed as part of Objective 3, below).

As an additional component, we were interested in evaluating reduction potential (as measured by platinum electrode) as a proxy for reaction rate. As discussed above, this approach is thermodynamically reasonable, although it has not generally been a useful approach based on reduction potentials measured in wells at field sites. However, we believed that a correlation between reduction rate and reduction potential was possible if the quality of the reduction potential measurement could be increased by utilizing soil slurries and electron shuttles to facilitate direct contact between suspended aquifer materials and the electrode. The approach is shown conceptually in Figure 1.2. Reaction rates for CT were measured in custom “rolling tube

reactors" (RTRs), and reduction potential was measured in soil slurries within the RTRs at the conclusion of each experiment. As Figure 1.2 indicates, an appropriate electron shuttle was added to the slurry to facilitate good contact between the electrode and particle surfaces.

Field samples were collected from 7 locations at 4 DoD sites (Indian Head, MD, Site 17 Naval Support Facility; St. Louis Ordinance Plant OU1, MO; F.E. Warren AFB, WY, Spill Site 7; and Site 45 Parris Island MCRD, SC). The methodology for cryogenic core collection at three

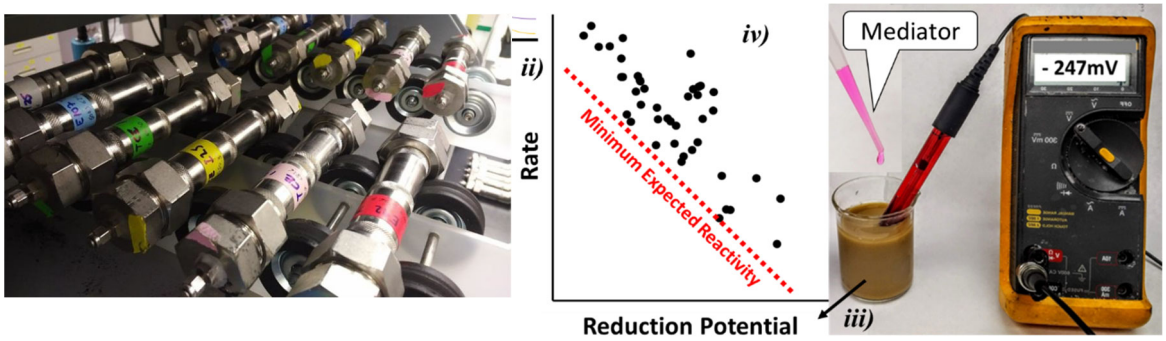

Figure 1.2. Schematic representation of data collection and analysis to assess the relationship between measured reduction rates and reduction potential.

of these sites has been well documented in previous SERDP and ESTCP reports (Sale et al., 2016; Olson, et al., 2017; Mattes, 2019).

Objective 3 - Determine if one or more of the RPs can provide robust measures of contaminant degradation rates using cryogenically-collected core samples.

As discussed above, there were two primary tasks for this objective. The first was the development of a predictive equation for reduction rate based on reduction potential and pH measurements. The second was the evaluation of the effects of freezing and storage on abiotic reaction rates. For the first task, data from Objective 2 were analyzed using a multiple linear regression approach based on Equation 1.3 to produce an equation for prediction of $\log(k_M)$ based on measured reduction potential and pH.

To evaluate the effects of freezing and storage on abiotic reaction rates we used materials from the two laboratory columns. Following the experiments conducted as part of Objective 1, the columns were disassembled, sectioned and the sections homogenized for use in a series of batch experiments that involved freezing and storage. To accomplish this, the homogenized samples were divided into multiple ~20 g subsamples. Those subsamples were separated into three groups and subjected to: 1) immediate reactivity testing; 2) freezing using liquid nitrogen, followed by thawing and reactivity testing; and 3) freezing and storage for 60 days prior to thawing and reactivity testing. The RTR reactivity procedure described for the field samples was used in these experiments. Disappearance of the parent compound (CT) and appearance of

reaction products were tracked over time. To assess the effects of freezing and storage, the analytical data were fitted to first-order rate expressions, and the modeled rates for the three sets of conditions were compared by taking the ratios of the modeled rates for the frozen and frozen+stored cases and dividing them by the unfrozen rates. All experiments were run in triplicate.

1.D. Results and Discussion

Objective 1 – Demonstrate the utility of reactivity probes over a range of geochemical conditions

Measurement of TCE and CT reduction rate in laboratory columns

As part of our effort to identify reactivity probes, we examined TCE and CT reduction in the two laboratory columns under stopped-flow conditions (Figures 1.3 and 1.4). Figure 1.3 shows that nearly 1000 hours were required to reduce the TCE concentration by an order of magnitude in both the magnetite (M1) and magnetite+sulfate (S1) columns.

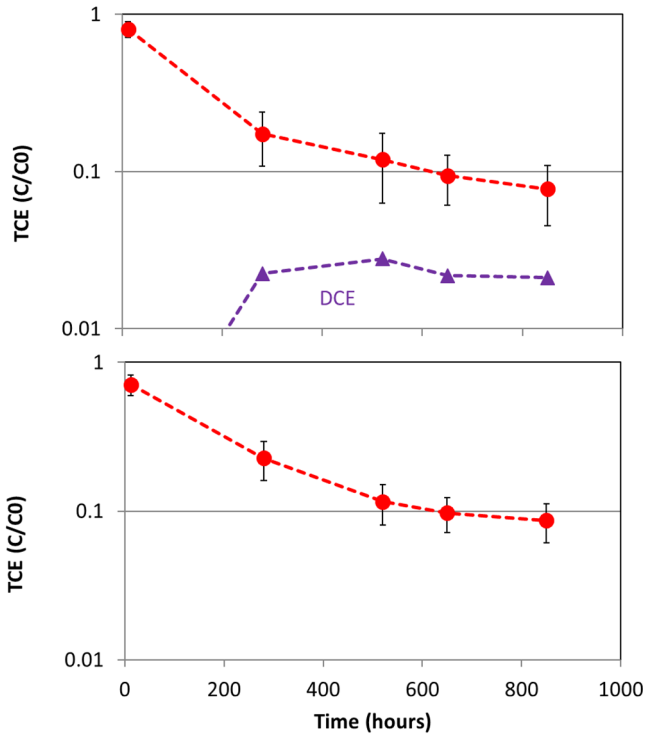

Figure 1.3. TCE degradation and DCE production in the magnetite (upper) and sulfate (lower) columns. All concentrations are normalized to the starting TCE concentrations.

For CT, concentration dropped ~3 orders of magnitude in under 100 hours (Figure 1.4). The CT also produced reduction products that were different for the two columns (CO in the magnetite column and CS2 in the column to which sulfate was added.) Another important result was that the reduction rate for TCE slowed substantially during the course of the 850 hour experiment, suggesting that the availability of the reactive mineral phases had decreased. For all of these reasons, it was determined that CT was the preferred reactivity probe for the subsequent experiments.

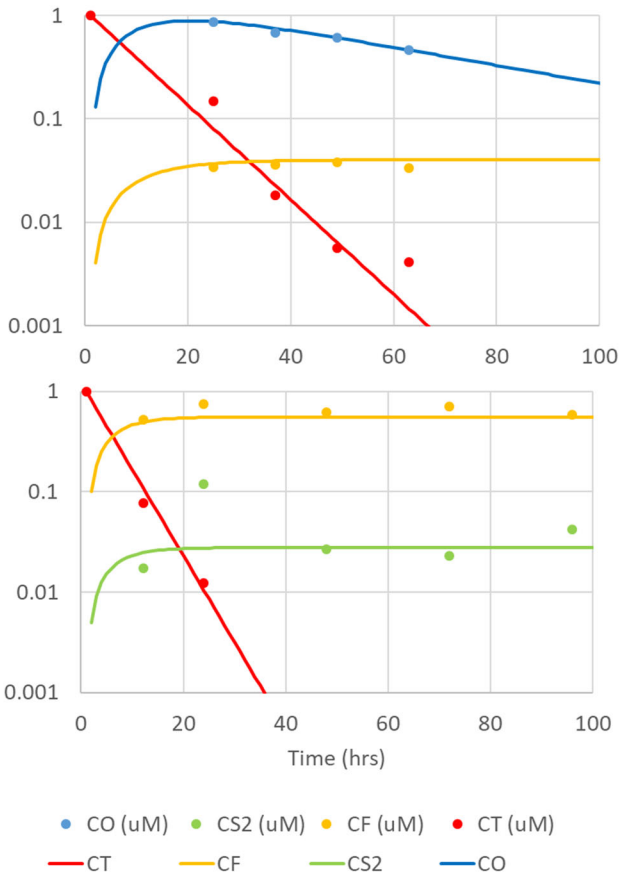

Figure 1.4. CT reduction and product formation in the magnetite (upper) and sulfate(lower) columns. All concentrations were normalized to the starting CT concentration in each experiment.

Objective 2. Measure abiotic reaction rates of actual field samples collected with the cryogenic core method

Soil cores from the four field sites were tested using batch experiments with our RTR system. The CT reactivity experiments generally took less than 100 hours for sufficient reduction to occur that rates could be determined. As part of our reactivity testing protocol we also measured reduction potential of soil slurries using an electron shuttle. This dual analysis allowed us to directly compare reactivity and reduction potential on the same sample. Those data are shown in Figure 1.5. (pH was also measured and will be discussed in Objective 3.)

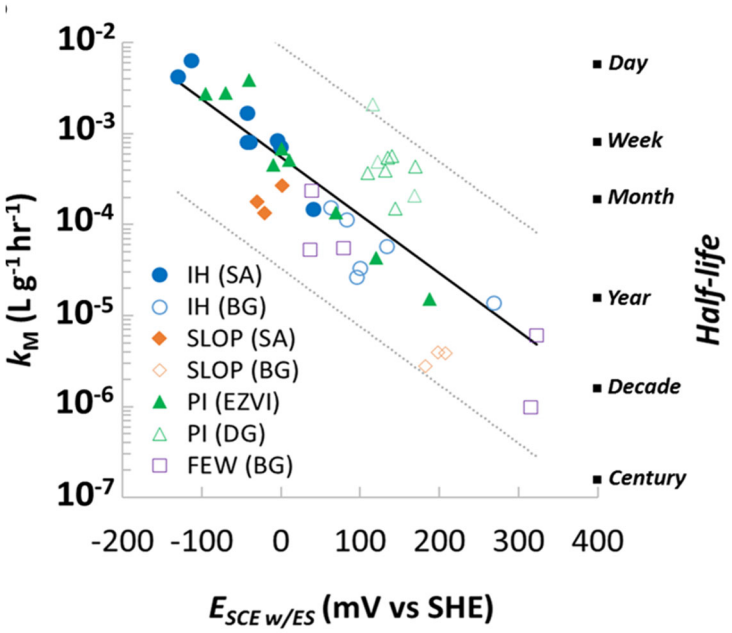

Figure 1.5. Correlation between measured mass-normalized CT reduction rate constant and reduction potential for samples

There are a number of interesting aspect of this figure. The first is that a single correlation is generally acceptable for all locations at all sites, despite differences in geochemistry at the sties. The second is that reaction rates at both source area and background sites show a similar relationship with reduction potential. These data point not only to the validity of the fundamental relationship between reduction potential and rate, but also to the possibility that similar reactive mineral intermediates may control abiotic reactions at a wide range of site types.

Objective 3 - Determine if one or more of the RPs can provide robust measures of contaminant attenuation rates using cryogenically-collected core samples.

As discussed above, prediction of reduction rates for field samples is an important goal of this project. Using the data from Objective 2, including pH and reduction potential, we applied multiple linear regression to fit the data to Equation 1.3. The resulting expression was

$$\log(k_M) = 0.178pH - 0.358\left(\frac{E_{ES}}{0.059}\right) - 4.662 \qquad [1.4]$$

where E_{ES} designates that an electron shuttle was used to make the potential measurement.

Using Equation 1.4 we can compare measured reaction rates measured in the batch tests to the model predictions based on Equation 1.4. Generally this approach provided order-of-magnitude or better estimates of rate based on combined pH and reduction potential measurements (Figure 1.6).

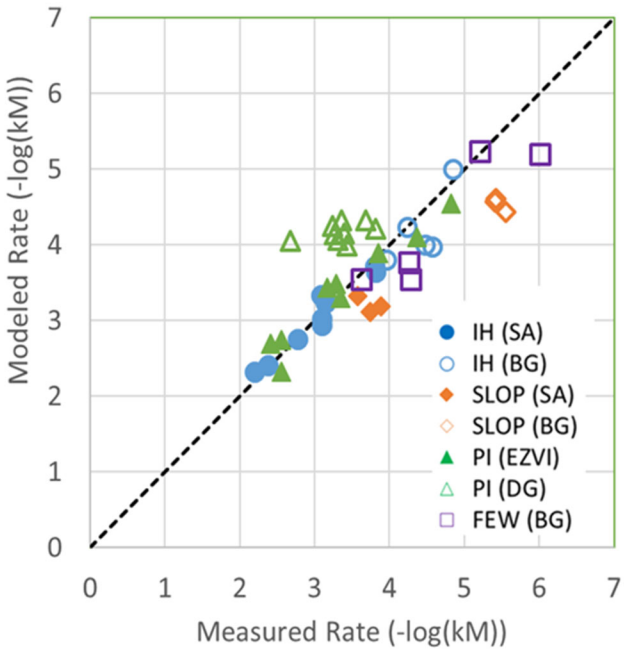

Figure 1.6. Measured and modeled mass-normalized CT reduction rate constants for the field data collected as part of Objective 2.

Effects of freezing on reaction rates in batch experiments using column materials

While the previous result is promising, it is important to examine the representativeness of the rates measured on core samples that have been frozen and stored. To accomplish this, samples from each section of each column for both columns were treated to three sets of conditions (unfrozn, frozen, frozen+stored). Each condition for each column section was analyzed in triplicate (54 individual experiments) using the RTRs. First order rate constants for CT disappearance, CF and CS2 appearance, and CO appearance and disappearance were determined for each experiment.

To assess the effects of freezing (T1) and freezing+storage (T60), the rate constants from each individual experiment were divided by the rate constant from the unfrozen case (T0). These data were combined to determine the average ratios for each reaction (e.g., for the kCT reaction, the T1/T0 ratios for all replicates from all column sections were averaged). The data in Figure 1.7 indicate that the measured rates for the frozen and frozen+stored samples were generally at or above the levels observed in the unfrozen samples (i.e., average T1/T0 and T60/T0 values are

greater than one). The CO production rate was an exception to this pattern. In addition, the measured rates for CO production were highly variable. We believe this was due, in large part, to the spatial variability of CO production and degradation within the columns. In the context of the modeling work discussed in the previous section, where order-of-magnitude estimates are expected, our conclusion is that freezing and storage do not adversely impact measurement of reaction rates.

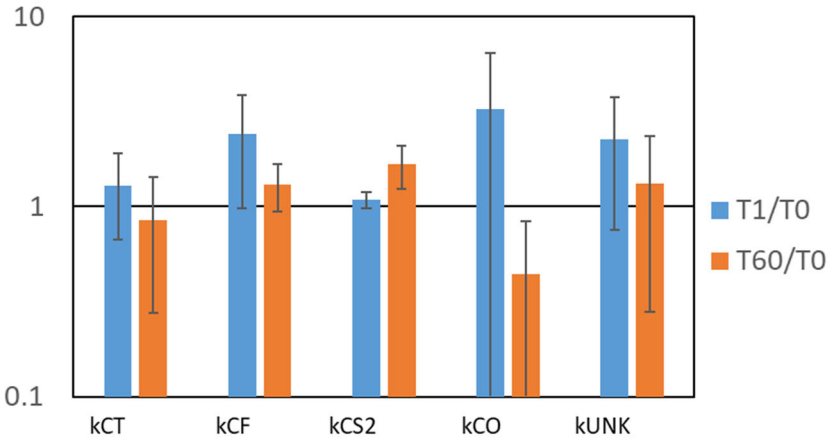

Figure 1.7. Average ratios of frozen to unfrozen (T1/T0) and frozen+storage to unfrozen (T60/T0) for the two laboratory columns.

1.E Implications for Future Research and Benefits

In summary, this work has resulted in three primary benefits for DoD and for groundwater restoration in general. First, we have demonstrated that CT works well as a reactivity probe for examining reduction rates at field sites. The reaction rates are sufficiently rapid to make laboratory experiments practical, and the reaction products can also be quite diagnostic. Furthermore, most sites have not been pre-exposed to CT and, as a consequence, reactions that occur immediately after initiation of batch experiments are a good indicator of abiotic reactions (i.e., no biological lag time).

Second, we have shown that the combination of reduction potential and pH can be used to predict measured rates to generally within an order of magnitude of the measured value. It is important to note here that the quality of the reduction potential measurement is key to this approach. Measurement of well-preserved core samples as slurries with an electron shuttle and, ideally with a well-characterized electrode, are critical to this success.

Third, freezing generally did not have a significant impact on measured reaction rates, so we believe that the approach of cryogenic core collection followed by laboratory measurements (either kinetic experiments or measurement of E_{ES} and pH) provide viable approaches for predicting abiotic reactivity of aquifer materials

These three conclusions come with several suggestions for future research. First, the method should be demonstrated with other contaminants in order to broaden the applicability of

the approach. Second, the current approach should be applied on a broader range of field samples, again to broaden applicability. Finally, identification of the RMIs that are active at field sites will be important in the context of how to insure long-term abiotic reduction.

2. Project Objectives

Three objectives were identified in the original proposal for this work. While these objectives have not changed, over the course of this project our understanding of the in situ formation of reactive phases has evolved significantly. This has led to a shift in the specific tasks completed to accomplish each objective. The tasks associated with each objective are briefly discussed in the sections below:

Objective 1. Demonstrate the utility of reactivity probes over a broad range of geochemical conditions.

The tasks undertaken to accomplish this objective evolved from a systematic study of commercially-available mineral phases to the use of laboratory columns to assess how biogeochemical conditions impact the formation of reactive minerals, which in turn control abiotic reactions. For this objective, we used two separate laboratory columns to create iron and sulfate reducing conditions, respectively. The two columns were operated for ~3 years during the project. One received bicarbonate-buffered groundwater containing lactate and the other column received groundwater with bicarbonate, lactate and sulfate. These columns, along with laboratory batch experiments, were used to evaluate a suite of reactivity probes (RPs) for use in estimating reduction rates.

Objective 2. Evaluate the use of RPs to measure abiotic reaction rates of actual field samples collected with the cryogenic core method.

Based on the reactivity probe selection in Objective 1, we used batch experiments to examine field reduction rates in samples from seven locations at 4 DoD facilities.

Objective 3. Integrate the data from the first two objectives to determine if one or more of the RPs can provide robust measures of contaminant degradaton rates using cryogenically-collected core samples.

An important goal of this project was to determine if high-quality soil cores could be used to estimate reactivity. The reactivity probe used in the first two objectives and high-quality reduction potential measurements represent two independent means of predicting reactivity. pH is also likely to affect rate, and in this objective we used measured reduction rates, reduction potentials and pH to evaluate a predictive equation for reactivity.

A second important task for this objective was to assess the effects of freezing and storage on measured reaction rates of core samples. As has been discussed elsewhere, cryogenic core collection has been demonstrated as a practical means of collection and preservation of field samples. However, the ability of freezing to preserve abiotic reactivity has not been demonstrated. To accomplish this, materials from the columns used in Objective 1were tested under a several freezing and storage conditions to examine the effects of freezing and storage on reactivity.

3. Background

Restoration of contaminated groundwater, particularly at geologically complex sites, is a complicated, time-consuming and expensive process (SERDP/ESTCP, 2018; Macdonald, 2000; Brown et al., 2007). At the same time, it is recognized that abiotic natural attenuation (ANA) processes can play significant roles in groundwater restoration, and in many cases can be enhanced by manipulation of subsurface conditions. However, these naturally-occurring processes are generally slow and are frequently complex, so our ability to characterize them is limited. As a consequence, SERDP recognized the need for additional tools to predict long-term performance via ANA, as well as engineered remediation, which led to the Statement of Need under which this project was funded (SERDP 2014).

Recent evidence suggests that the active formation of mineral phases is important for overall reactivity via ANA (e.g., Culpepper et al., 2018; Hyun and Hayes, 2009; Lan and Butler, 2016). Formation of these minerals is likely to be highly dependent on the localized (bio)geochemical cycling driven by dissimilatory iron and sulfur reduction and transformation of existing minerals. Under these circumstances, new mineral phases likely are continuously formed and consumed by biotic and abiotic geochemical processes. Because of their meta-stable nature, these materials have come to be known as "reactive mineral intermediates" (RMIs). RMIs likely include very high surface area amorphous solid coatings, and/or colloids and nanoparticles. The emerging conceptual model of RMIs is an important tool for understanding ANA processes and their potential for long-term treatment of contaminated groundwater.

3.A.The relationship between reduction potential and reduction rate

In remediation practice, measurement of reduction potential (E) of well-water samples has been widely used as a proxy abiotic reactivity. However, conventional E measurements on water-only samples have generally proven unsuccessful for prediction of contaminant reduction rates in groundwater. This is now believed to be the case because those groundwater measurements do not accurately reflect reduction potential at the mineral surfaces on which the reactions occur. Stewart et al. (2018) recently developed a correlation equation between contaminant reduction rate, pH, and reduction potential. Their general equation for this relationship was:

$$\log(k_{SA}) = \mathrm{a}\left(\frac{E}{0.059}\right) + b\ \mathrm{pH} + c \qquad [3.1]$$

Where k_{SA} is the surface-area normalized rate constant for a reaction, and a, b, and c are constants characteristic of that reaction.

For field samples composed of mixed mineralogy, reactive surface areas (SSA_R) cannot be measured, so we have transformed equation (1) into the mass-normalized version, where the term *c'* is a constant that also contains the unknown reactive surface area for the sample.

$$log(k_M) = a\left(\frac{E}{0.059}\right) + b\ \text{pH} + c + \log(SSA_R) \quad [3.2]$$

$$\log(k_M) = \text{a}\left(\frac{E}{0.059}\right) + b\ \text{pH} + c' \quad [3.3]$$

For a given field site, it may be reasonable to assume that the reactive mineral phase, SSA_R, and soil to water ratio (M, g L^{-1}) are relatively constant, and thus a linear relationship between E and log (k_M) might be expected. However, across a range of field sites it is expected that these values could vary significantly. Consequently, the hypothesis that Equation 3.3 is applicable across multiple field sites needs to be rigorously tested. To accomplish this, accurate measurements of rate constants, pH and reduction potentials would be required. Because the role of mineral surfaces is important, well-preserved field samples (e.g., cryogenic core collection) will be required for both the measured abiotic reaction rates and reduction potentials. Furthermore, accurate measurement of reduction potentials requires intimate contact between the measurement electrode and those mineral surfaces. Electron shuttles (ESs) have emerged as one approach to improve reduction potential measurements of heterogeneous media and have been adopted in growing array of conditions following their demonstration for model iron minerals (e.g., synthetic iron oxides with sorbed Fe^{2+}). This study demonstrates the utility of high-quality ES-based reduction potential measurements using cryogenically-collected field cores to predict abiotic reduction rates.

3.B. Role of microbiology in controlling subsurface geochemistry

It is widely recognized that microbiology serves as an important source of reduced mineral phases in the subsurface (e.g., Fe^{2+} and S^{2-} based minerals). As discussed above, it is also widely recognized that those phases can either form new mineral phases (e.g., FeS, $Fe(OH)_2$) or sorb to existing mineral phases. In both cases, laboratory data indicate that abiotic reduction of chlorinated hydrocarbons can be significantly enhanced (e.g., Culpepper, 2018). As a consequence of our evolving understanding of abiotic processes, our understanding of the role of RMI phases has also evolved significantly in the last 5 years. A key in this regard is our understanding of the meta-stable nature of many of the important RMIs. For species like FeS, a continuous source of iron and sulfide is required to sustain those minerals, and that in turn requires ongoing microbiological production of the precursor species.

3.C. Effects of freezing and storage on reactivity

The utility of using cryogenically collected core samples and laboratory based measurements of reduction rates and reduction potentials for predicting in situ reactivity has not

been demonstrated. As part of two SERDP projects we have evaluated the efficacy of collecting soil cores by freezing them in situ prior to recovery to ground surface. The initial motivation for our cryogenic core sampling work came from the need to collect core samples for molecular tools analysis (e.g., DNA, mRNA) as part of SERDP ER-1559 (Johnson, 2012). That work demonstrated the ability to freeze and store core samples and then recover very-labile mRNA (half-life of ~1 hour at room temperature).

Freezing is the preferred approach for storing solids collected from anoxic environments (U.S.EPA, 2002). This approach has been show to preserve the redox integrity of reduced iron and sulfur-bearing compounds, which control abiotic attenuation behavior at hazardous waste sites. Wilkin (2006) compared sediment samples from a contaminated site stored under preserved (i.e., frozen) conditions and exposed to air. Analyses included total iron, ferrous iron, total sulfur and acid-volatile sulfides (AVS). Some of those data are shown in Figure 3.1 and indicate that both ferrous iron and AVS concentrations were dramatically reduced in the unpreserved (i.e., unfrozen) samples. It was also observed that the unpreserved sediments began to turn from black to red within a few hours of collection.

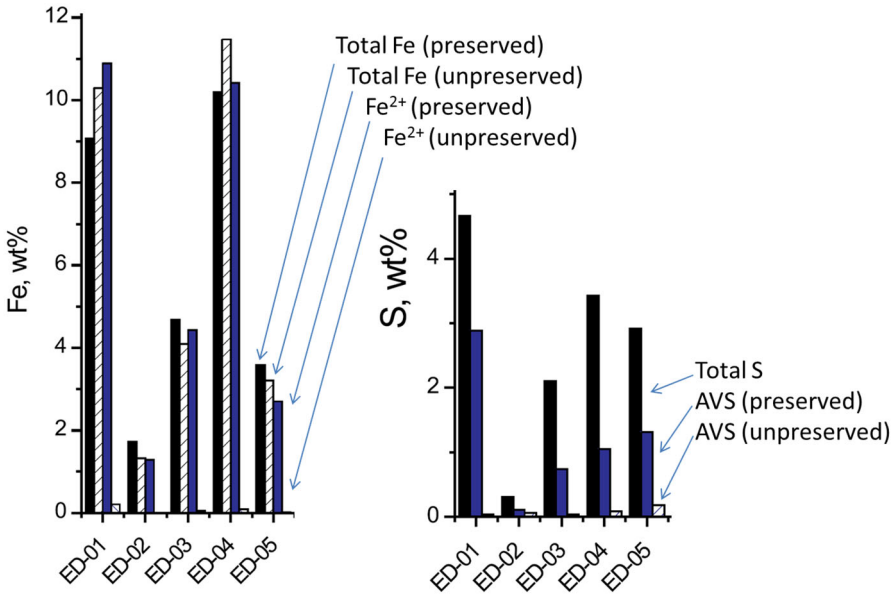

Figure 3. 1. Effect of preservation (freezing) on ferrous iron and acid-volatile sulfides in anoxic sediments (adapted from Wilkin, 2006)

However, this work did not discuss the possible effects of freezing on reactivity. As a consequence, in the work reported here we conducted a series of experiments to evaluate how freezing impacts measured rates of contaminant reduction. .

3.D. Reactivity probes for batch kinetic studies

Reactivity probes, as used here, are intended to provide rapid, reliable measurement of the ability of aquifer sediments to abioticly reduce CoCs. As a consequence, there are a number of properties of the probes that should be considered when optimizing for these measurements, including:

- Rapid reaction to facilitate batch tests
- Well-characterized reaction pathways
- Products diagnostic of reaction pathways
- Ease of analysis (e.g., for possible field application)
- Reactions occur primarily via abiotic pathways

We considered two classes of compounds for this work, redox-sensitive dyes and chlorinated hydrocarbons. There are a broad range of redox-sensitive dyes that are potentially useful. To be practical as probes, the dyes should be anions or neutrally charged in both their oxidized and reduced forms in order to minimize sorption. Ideally they would also be non-toxic and absorb in the visible light range to facilitate detection. Four commonly-used dyes that meet those criteria (Figure 3.2) are Resacurin (Res), Resorufin (Rsf), Indigo Disulfonate (I2S), and Indigo Tetrasulfonate.

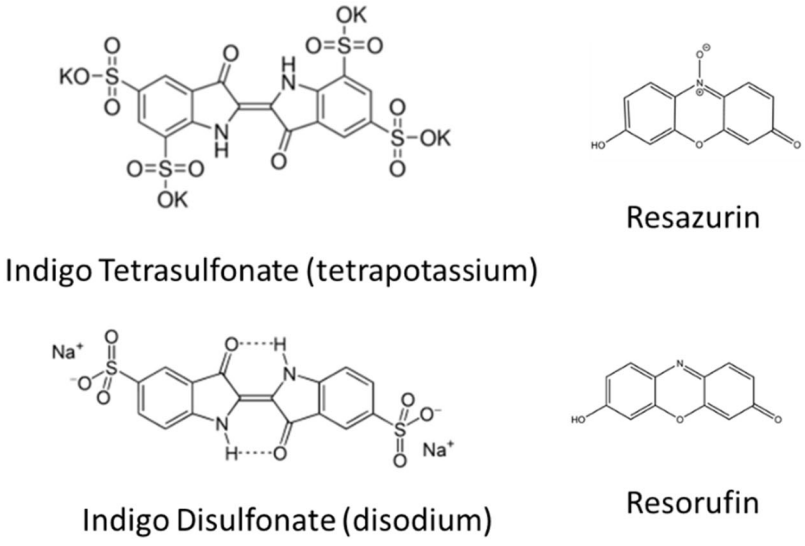

Figure 3. 2. Redox-sensitive dyes evaluated as reactivity probes in this study.

We have previously used these dyes as indicators and as reactivity probes to examine reduction rates by pure mineral phases (Fan et al., 2016; Tratnyek and Johnson, 2017). As the data in Figure 3.3 indicate, rates measured with the dyes can be quite rapid, even with relatively weak reductants like aqueous Fe(II) and goethite (GT).

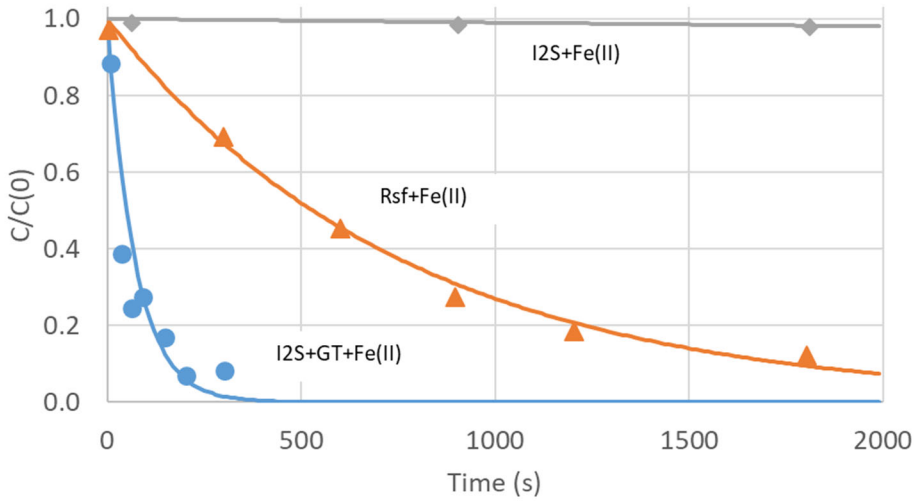

Figure 3. 3. Reduction of resorufin (Rsf) and indigo disulfonate (I2S) by aqueous ferrous iron (Fe(II) and goethite (GT). Adapted from Tratnyek and Johnson 2017.

Chlorinated hydrocarbons used as probes can include primary contaminants like PCE, TCE, or CT. They can also include chemical analogs like trichlorofluoroethene (TCFE). The analogs have the potential advantage that they are easily distinguished from the primary contaminants that might be present in field samples. Primary contaminants have the advantage that they provide a more-directly applicable rate measurement. However, a practical disadvantage of the primary contaminants is that, if present in the original sample, may have resulted in a microbial population capable of directly degrading the compounds, and thus complicating interpretation of abiotic rates.

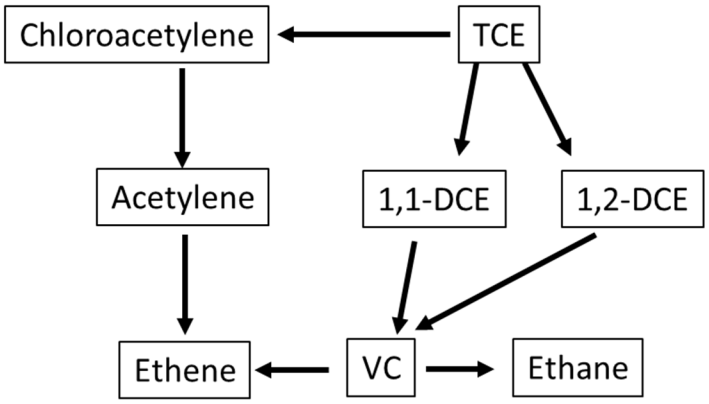

Figure 3. 4. Simplified schematic drawing for TCE degradation. Adapted from Butler and Hayes (1999)

TCE. Literature data for abiotic TCE degradation has generally identify two reductive pathways as being dominant (e.g., Butler and Hayes, 1999; Lee and Batchelor, 2004; McCormick and Adriaens, 2004). Figure 3.4 shows a simplified reaction scheme modified from Butler and Hayes (1999) and others. The production of chloroacetylene occurs via reductive elimination to produce chloroacetylene and hydrogenation results in the production of one of several dichloroethenes (DCEs, He et al., 2015).

Figure 3.5 shows data from the U.S.EPA (2009) for a test using TCE and sediments from the Twin Cities Army Ammunition Plant (TCAAP). As the data indicate, the timeframe for reactivity tests using TCE can be prohibitively long. Not only does this problematic from a decision support perspective, but it also carries with it the risk that the loss of reactive phases present at the time of collection may result in an underestimation of rates.

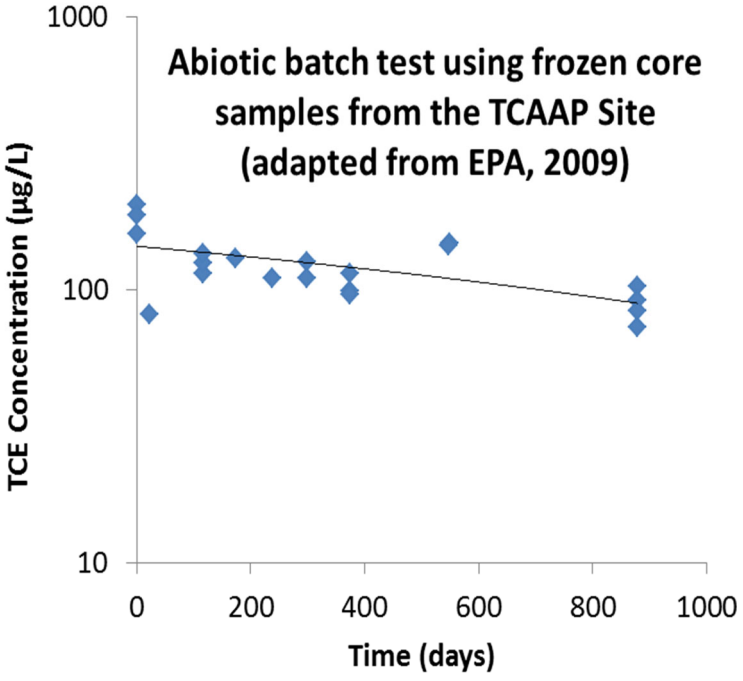

Figure 3. 5. Example laboratory batch test results for abiotic attenuation of TCE on aquifer materials (adapted from U.S. EPA, 2009)

TCFE. TCFE has been used in laboratory and field studies as a reactivity probe primarily for biotic systems where the microbial populations had been optimized for TCE reduction (Vancheeswaran, 1999; Hageman et al., 2001). In laboratory systems, essentially all of the TCFE was transformed via reductive dehalogenation with loss of chlorine atoms (Figure 3.6). There are no data available in the literature regarding TCFE reduction with mineral phases.

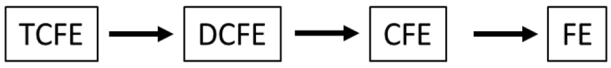

Figure 3. 6. Reaction pathway for biotic TCFE reduction. Adapted from Vancheeswaran et al., 1999

CT. There is a large body of literature on mineral-based abiotic degradation of CT (Elsner et al., 2004; Shao and Butler, 2009; Devlin and Muller, 1999; Danielson and Hayes, 2004; Kriegman-King and Reinhard, 1992). Multiple pathways with distinct products have been identified,

including CF, CO, CS2, CH4, formate. Most published reaction schemes are variations on the version published by Kriegman-King and Reinhard (1991), which is shown in simplified form in Figure 3.7.

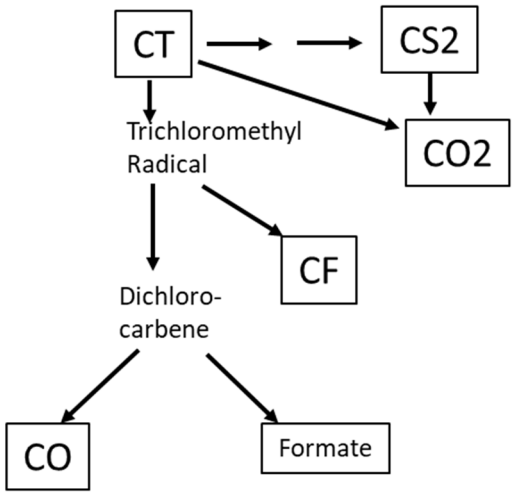

Figure 3. 7. Simplified reaction scheme for CT reduction. Adapted from Kriegman-King and Reinhard, 1991.

The major reaction products have been shown to vary significantly depending on the mineral phase present in the system. For example, Danielson and Hayes (2004) observed that CO was the major reaction product of the reaction between CT and magnetite. They also observed CF as a lesser product. CS2 is widely observed as a product of sulfur-based minerals, in particular FeS and FeS2. FeS tends to be meta-stable in the environment, converting to FeS2 over a period of months. Shao and Butler (2009) examined how reactions with CT changed during that process. They observed significant shifts in product formation when CT was reacted with FeS that had aged to different extents (Figure 3.8)

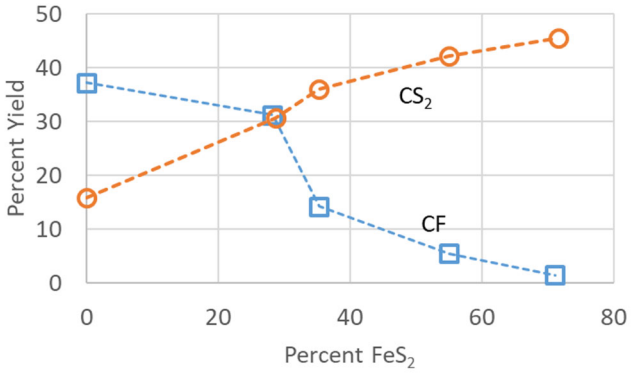

Figure 3. 8. Shift in reaction products for CT reduction as a function of the percent of FeS oxidized to FeS2. Adapted from Shao and Butler, 2009.

Based on literature data, the expected strengths and weaknesses of each of the redox dyes and chlorinated hydrocarbon probes discussed above are summarized in Table 3.1. Batch and column studies were used in the following sections to assess the utility of these reactivity probes under different geochemical conditions in laboratory columns and in field cores.

Compound	Rapid reaction to facilitate batch tests	Well-characterized reaction pathways	Products diagnostic of reaction pathways	Ease of analysis (possible field application)	Primarily abiotic reactions
Resorufin	X			X	X
I2S	X			X	X
TCE		X			
TCFE	?	X			X
CT	X	X	X		X

Table 3. 1. Expected strengths of reactivity probes examined in this study.

4. Materials and Methods

The materials and methods used in this project are summarized in the flow diagram below (Figure 4.1).

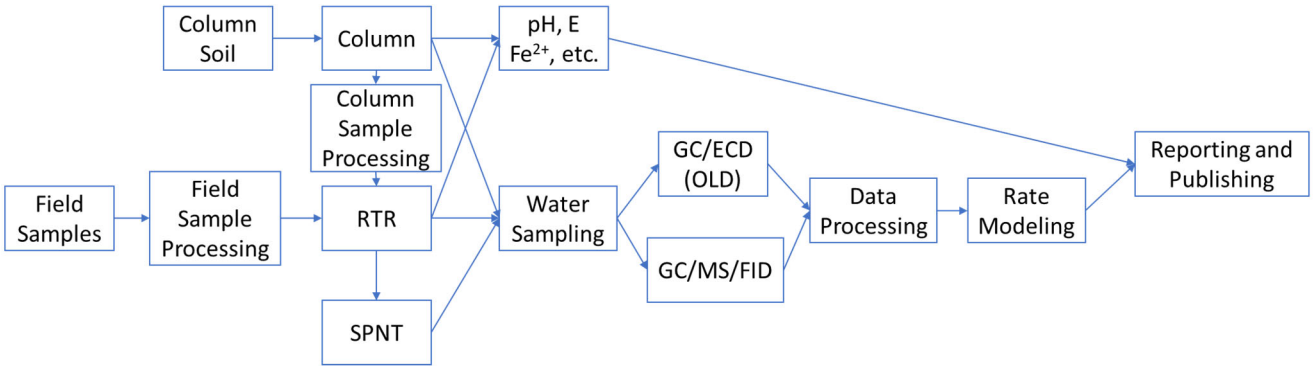

Figure 4. 1. Flow diagram of sample handling for laboratory column experiments and field core samples.

Each box is described in the subsections below. The cryogenic core collection method has been described previously (Sale et al., 2016; Olson, et al., 2017), and is only briefly covered here. Column operating conditions are typical of other experiments, but the details required to replicate the experiments are presented. Batch experimental rate constant measurements were made using custom built "Rolling Tube Reactors" (RTRs), and the details of their design are provided below. Water sampling and analysis via headspace analysis are relatively straightforward. During the project, with the support of SERDP, our analytical capabilities were significantly upgraded with the addition of a custom designed GC/MS/FID system, and the configuration of this instrument is described in the analytical section.

4.A. Soil Columns

The soil columns used in Objectives 1 and 3 are shown in Figure 4.1 They were constructed out of polycarbonate and had dimensions of 42 cm long and 5 cm inside diameter. They were filled with naturally-sourced Columbia River sand, to which had been added 1% by weight 60-80 mesh magnetite (Prospectors Choice, Surprise, AZ). The final porosity of the columns was about 40%. The columns were mounted vertically and were operated in an up-flow mode.

Four sampling ports were located 6, 16,26, and 36 cm along the flow path. Each of those sampling ports was composed of a nylon pipe reducer, a 1/16" tube to 1/16" pipe Swagelok connector and a #16 hypodermic needle (see insert in Figure 4.2)

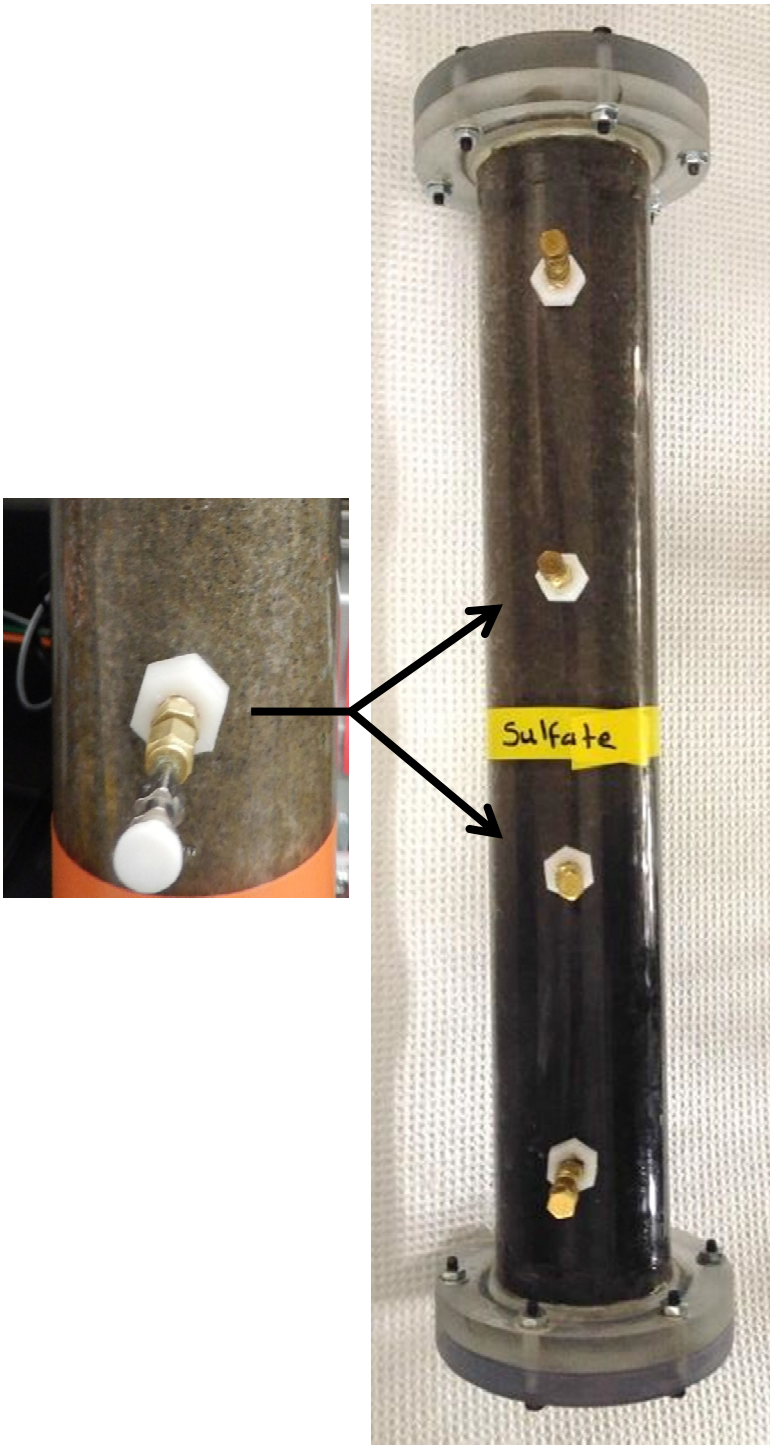

Figure 4. 2. Photographs of one of the soil columns used for this project. The insert shows detail of the sample port construction, which is further described in the text.

Groundwater chemistry – The synthetic groundwater flowing into the columns was buffered with 6.4 mM sodium bicarbonate that was adjusted to pH=7.2. Lactate was also added to the influent groundwater (10 mM). For the sulfate column, sodium sulfate was added to achieve a final concentration of 14 mM. Prior to injection, the groundwater was stripped of oxygen (and some carbonate) using a counter-current stripper with nitrogen gas.

Groundwater flow control – Flow in the column was controlled using ceramic-piston pumps (Fluid Metering, Inc. Model H0CKCLF pump heads.) The flow rate through the column was ~30 mL/hr. With an internal volume of ~830 mL and a pore volume of ~360 mL, that corresponds to a residence time of approximately 12 hours.

Geochemical sampling – For geochemical measurements, water was periodically removed from the columns via the Luer fitting ports at the 4 locations along each column (6, 16,26, and 36 cm down the column). For sampling of geochemical parameters, 1 to 10 mL of water (depending on the type of analysis) was removed from the column using a syringe, after letting ~0.5 mL flow out of the port to flush it. The analytical methods used for the geochemical parameters are discussed below.

Contaminant/reactivity probe introduction – Periodically, TCE or CT (along with TCP as an internal standard) were introduced into the column. This was accomplished using a syringe pump and a water reservoir containing a saturated solution of a 2:1 (by volume) of (CT or TCE): TCP. To deliver the RPs, a 60-mL syringe filled with water was connected to the reservoir the syringe pump was set at 0.5 mL/hr. Water flowing from the syringe displaced stock solution from the reservoir and delivered it to the influent line of the column. The resulting concentrations were ~450 uM for CT and ~87 uM for TCE

Contaminant/Reactivity Probe sampling – As with the geochemical measurements, 1 mL of water was removed from the column ports with a syringe for analysis. In this case, the water was immediately injected into a sealed 20-mL headspace vial for analysis (discussed below)

Column soil processing – At the conclusion of the column experiments, the columns were disassembled and the soils used for subsequent analysis. To accomplish this, the columns were capped and cut into four sections, centered around each sampling port, with a reciprocating saw. The column sections were quickly covered with aluminum foil and transferred to an anaerobic glove box. Once in the glove box the core material was removed from a polycarbonate column section and thoroughly mixed. The mixed sample was then divided into ~20 gram subsamples for subsequent analyses. Each subsample was wrapped in clean aluminum foil.

4.B. Field Samples

Selection of Field Sites for Sampling. The main criteria for samples selection was the availability of samples that could be cryogenically collected or preserved immediately upon collection. However, it was also important to represent a cross section of the DoD cleanup objectives and include commonly used remediation amendments in the site samples. Four sites were selected for analysis and are summarized in Table 4.1**.** Background samples were collected where possible at all the chosen sites. Additional background samples were selected at F.E. Warren Air Force Base, Wyoming where previous SERDP and ESTCP demonstration projects have taken place. Two soil mixing sites were selected (Indian Head, Maryland and St. Louis Ordinance Plant (SLOP), Missouri) and one emulsified zero valent iron (EZVI) site (Parris Island, South Carolina) to provide a context for our analysis under engineered remediation conditions as well as the pertinent background conditions, where possible. These sites underwent remediation 5-11 years prior to sampling and represent conditions in various states of aging and were expected to exhibit a corresponding range of reduction kinetics.

Sample Collection and Preservation in the Field. The cryogenic core collection method used in this study was developed during a previous SERDP project (ER-1740) and has been described in detail previously (Sale et al., 2016, Kiaalhosseeni et al., 2016; Johnson et al., 2012; Brow et al., 2010).

In this study, cryogenic core collections were performed by Drilling Engineers Inc. (Ft. Collins. CO) using a truck mounted hollow stem auger and continuous sample tube system modified to allow for injection of liquid nitrogen into a dual-walled cooling cylinder. Rapid circulation of liquid nitrogen ensured fast-freezing in the polyvinyl-chloride sleeves, which resulted in greater than 95% recovery in all media, thereby enabling high throughput and high resolution core analysis for multiple analytes. Cryogenic core collection and preservation has been previously shown to provide preservation for microbial analytes (Johnson et al., 2012; Brow et al., 2010) and the rapid freezing prevents redistribution of analytes within the sample matrix, providing the highest quality preservation available for ex situ analysis (Wilkin, 2006). Samples from the IH and SLOP sites were collected by collaborators through ESTCP grant numbers ER-201589 (Olson et al., 2017) and ER-201587 (Popovic et al., 2018), Samples from the PI site were collected in collaboration with ESTCP Project ER-201425 (Mattes, 2019). FEW site samples were collected at the same location reported by Sale et al. (2016).

Sample Processing in the Laboratory. To preserve in situ conditions as much as possible, the cryogenically collected cores were stored in a -20º C freezer until experiments were started. Handling times of frozen samples outside the anoxic chamber was limited to 5 min in a walk-in fridge at 15º C. During experimental preparation the sample's exposure to the atmosphere was limited by the use of an anoxic chamber (high purity N_2, <0.2 ppm O_2). Frozen samples were cut into 1 inch thick "hockey pucks" using a chop saw with diamond blade. Figure 4.3 illustrates further sample processing of frozen soil puck. Pucks were then segmented using a mallet and

mason's chisel on a cutting board (A). Subsamples from this puck are considered to be a single sample and were portioned from the puck (B); for analysis into pre-weighed vessels for analysis streams described below for potential measurements in electrochemical cells or experiments in specialized the kinetic experiment apparatus (C), described below.

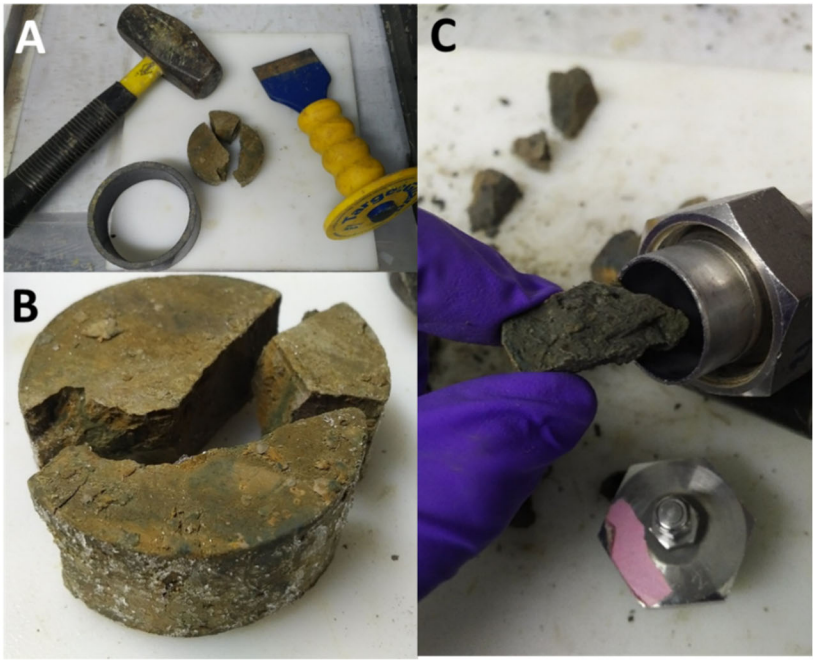

Figure 4. 3. Photos of sample processing of cryogenically stored material and preparation of kinetic experiments. (A) Frozen material was split using a chisel and mallet and (B) subsampled from one inch. frozen puck sized pieces that are cut from a soil core. (C) Rotating Tube Reactors (RTRs) and electrochemical cells are loaded with frozen pieces of sample before being sealed. Processing time was kept under 2 mins of exposure to minimize passivation (oxidation) of mineral species. All of these steps were performed in a cold room at 4^{o} C

Location, References (more information)	Site	Remediation Activity	Site Description	Sample Locations
Marine Corp. Recruit Depot, Parris Island, SC [7-10]	Site 45	EZVI injection RNIP and vegetable oil.	Silty-Sand, PCE spills spanning several decades.	(EZVI) BH1 – EZVI injection zone, PCE NAPL contamination
				(DG) BH2 – 10 m downgradient of EZVI Inj.
				(DG) BH3 - 20 m downgradient of EZVI Inj.
				(DG) BH4 – 30 m downgradient of EZVI Inj.
Naval Surface Warfare Center - Indian Head, MD [5, 6]	Site 17	ZVI-Clay Soil-mixing amended soil.	Lowland reducing sediment, high in organics, clayey-silt.	(SA) Source area – ZVI-clay soil mixing zone
				(BG) DG2A – background samples in untreated area – high VOC conc.
				(BG) DG2B – background samples in untreated area – low VOC conc.
St. Louis Ordinance Plant, St. Louis, MO [5]	OU1	ZVI-Soil mixing, GMA ZVI	Oxidized silty-sand sediment.	(SA) SB001 – soil mixing zone in a previous source area
				(BG) SB003 – background samples outside of treatment zone
F.E. Warren AFB, Cheyenne, WY [1]	Spill Site 7	Downgradient of ZVI PRB – TCE plume	Semi-consolidated silt, moderate degree of calcification.	(BG) Background samples from one borehole profile

Table 4. 1. . Summary of field sites, sampling locations, and conditions

4.C. Chemical Measurements

Batch Reactor Design. Custom Rolling Tube Reactors (RTRs) were used to for the abiotic degradation rate experiments. The RTRs (Figure 4.4) were manufactured from polished 316L stainless steel. The wide openings at the ends of the RTR allowed loading of cryogenic samples directly, minimizing sample disturbance and thawing. During sample processing, cryogenic core material was loaded into an unsealed RTR (Figure S1C), capped and sealed except for one end plug, then passed into an anoxic chamber by purging the anti-chamber 4 times with nitrogen. The RTRs were flooded with deoxygenated 6.4 mM bicarbonate buffered solution to remove headspace using Luer-to-1/16th Swaglock stainless steel adaptors on both ends, sealed completely in the anoxic chamber, and then passed out of the anoxic chamber, mixed overnight at 6 rpm using a custom-made roller (shown in Figure 4.5).

The sample and fluid masses in the RTRs were determined gravimetrically throughout the process.

Figure 4. 4. Photograph of disassembled Rolling Tube Reactor

Figure 4. 5. Rolling Tube Reactors (RTR) reactors used for the kinetic studies. Here they are shown on the roller system that rotated them at ~10 revolutions per minute

Once cryogenic core samples are loaded into the RTRs, they are positioned vertically, flooded with buffered water from the bottom, and placed on custom rollers (Figure 4.5). In order to sample the RTRs they must again be hung to vertically to allow for fluid displacement from bottom to top using syringes.

Contaminant Degradation Rate Experiments. One mL each of aqueous stock solutions containing saturated carbon tetrachloride (CT) and trichloropropane (TCP, internal standard) were introduced into the RTR by injection through the Swagelok fitting, displacing one mL of buffer solution from the top of the tube. Once mixed, the target starting concentrations were ~53 µM for CT and ~230. µM for TCP. Preliminary experiments using RTRs and field sediment show no significant loss of TCP over 500 hours. Therefore, TCP is appropriate to use as an internal standard for subsequent experiments. Additionally the TCP can also be used to automatically account for dilution as a result of the sampling process.

To sample the RTRs, one mL of deoxygenated, bicarbonate-buffered water was injected via syringe into the bottom of the vertically-mounted RTR, displacing one mL from the top of the RTR into a second syringe. The displaced fluid was then injected into a 20-mL headspace vial which had been sealed in an anoxic chamber to eliminate atmospheric gases.

Reduction potential and pH measurement of RTR samples. At the conclusion of each RTR experiment, the RTR was hung on a rack, the upper cap removed, and a combination platinum electrode (MI-800-411B, Microelectrodes Inc, Bedford, NH) was used to determine the reduction potential. An electron shuttle (ES) was then introduced into the tube (20 µM indigo tetrasulfonate or indigo disulfonate, TCI America, Portland, OR), and the reduction potential was

monitored until a stable value (E_{ES}) was reached. The performance of the platinum electrode was demonstrated by comparison to an electrochemistry-grade rotating disk electrode (Kocur et al., 2020). Concurrent with the E_{ES} measurements, the final pH of the experiment was determined using a combination pH electrode (Vernier Software and Technology, Beaverton, OR)

Field protocol for measuring potential in field samples

This reduction potential measurements in the RTRs described above was the genesis of a simple but robust field reduction potential measurement protocol that can be readily integrated into routine field monitoring program. A preliminary field protocol is shown in **Figure 4.6**, which includes 5 steps: 1) place a sub sample of soil core in a vial; 2) add distilled water to the vial and mix the vial to form a soil slurry; 3) measure the *E* of the slurry using a calibrated combination platinum electrode; 4) add an appropriate electron shuttle to the slurry and re-mix the vial; and 5) measure *E* again after an elapsed time.

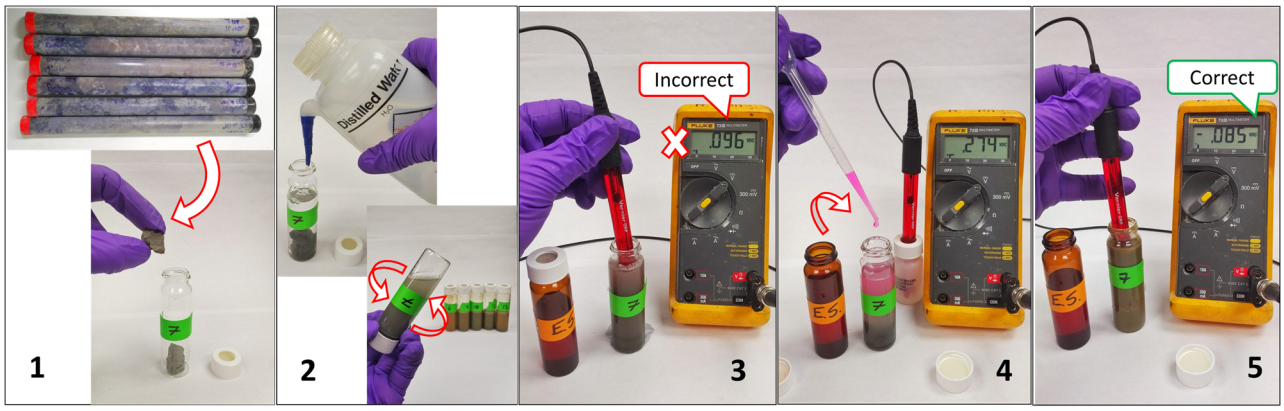

Figure 4. 6. A preliminary field protocol of the ORP Kit. Comparison between the meter readings between Steps 3 and 5 shows that ORP of the soil slurry changed from + 96 to −85 mV after addition of an aliquot of electron shuttles.

The field protocol presented here is a simple procedure that can be easily carried out in the field with minimum training, although further assessment will be needed to determine it's robustness.

Gas Chromatographic Analysis of Contaminants/Reactivity Probes. GC/ECD Measurements – For approximately the first half of this project, determination of TCE, CT and TCP concentrations, as well as chlorinated reduction products, was accomplished using a Hewlitt Packard 5790 gas chromatograph with an electron capture detector (GC/ECD). Calibration of the GC/ECD was accomplished using external standards prepared from a known stock solution. All calibration and sample analyses were performed by extracting a volume of headspace (~100 uL) out of the 20 mL sample vial that contained a 1 mL water sample.

The calibration stock solution was contained in a sealed 2-L bottle with a pair of Luer fittings on the top. The bottle contained DI water to which known masses of a suite of analytes

had been added. One mL of the stock solution was displaced out of the bottle with 1 mL of DI water. The stock solution is depleted by ~0.05% in this process, resulting in a ~3% reduction over 60 events. Daily response factors were tracked and the stock solution was replaced as needed.

GC/MS/FID Measurements – Midway through this project, with the support of SERDP, we obtained a custom-designed GC/MS/FID system. This instrument has the capability to analyze a broad range of contaminant compounds and reaction products in a single-injection analysis using a dual-column configuration. For this project, the list of available analytes is shown in Table 4.2. The system is automated with an RSI 85 autosampler (PAL Systems, Zwingen CH), which injects a 0.1 mL headspace sample into a customized Agilent 7890B GC. Initial separation of respiration gases from chlorinated and other analytes is performed on a DB-624 Ultra Inert column (0.25 mm ID, 30 m, Agilent, Santa Clara, CA) at 35 C. A switching valve directs the respiration gases to a carbonPLOT column (0.32 mm ID, 30 m, Agilent, Santa Clara, CA) for further separation. Compounds eluting from the carbonPLOT column pass through a nickel-catalyzed methanizer, where they are all converted to methane or ethane. Simultaneous with the activation of the switching valve, the oven temperature is increased from 35 C to 175 C at a rate of 20 C per min. Effluent from the DB-624 column are directed to the mass spectrometer (5977B MSD, Agilent, Santa Clara, CA).

FID analytes	MS analytes
CO	Chloromethane
CO2	Dichloromethane
CH4	Chloroform
Ethane	Carbon Tetrachloride
Ethene	Chloroethene
Acetylene	Dichrlorethene
	Trichlroethene
	Hexachloroethane

Table 4. 2 Analytes used in this project detected with the GC.MS/FID method

4.D. Modeling

Kinetic data fitting

Based on literature data, the following reaction scheme was used to model kinetic data for the field samples and for the columns and column soils (Figure 4.7). This approach makes the implicit assumption that, even though there may be common intermediates for more than one of the products, the rate-limiting step for each product is unique to that product. (This assumption is borne out in our experimental data).

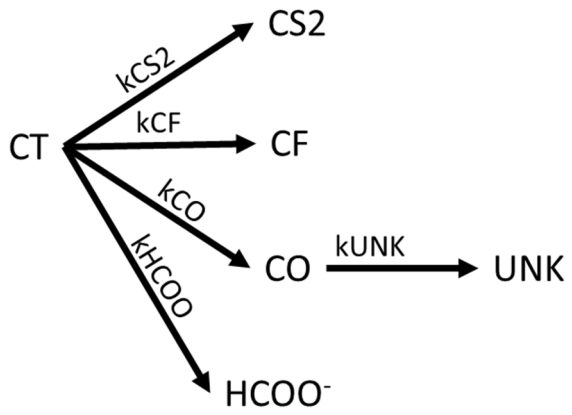

Figure 4. 7. Reaction scheme used for modeling.

The observed rate constants for CT disappearance, and the appearance of CS2, CF and CO were determined using explicit finite difference solutions to the rate equations:

$$d[CT]/dt = -kCT*[CT] \quad [4.1]$$

$$d[CF]/dt = kCF*[CT] \quad [4.2]$$

$$d[CS2]/dt = kCS2*[CT] \quad [4.3]$$

$$d[CO]/dt = kCO*[CT]-kUNK*[CO] \quad [4.4]$$

For the purposes of this analysis it was assumed that the rate for formate formation (kHCOO), which was not measured, could be calculated from observed the observed rates for the disappearance rate of CT and production of CS2, CF, CO, such that:

$$kHCOO=kCT-(kCS2+kCF+kCO) \quad [4.5]$$

To facilitate comparisons between column experiments and field samples, all rate constants reported here are expressed as mass-normalized values (i.e., observed rate constant divided by the soil to water mass ratio, with resulting units of mL/hr/g)

Multiple linear regression of pH, E and rate constant data

To develop a predictive equation for CT reduction rates for the field samples, a least squares multiple linear regression approach was developed using Labview software (NI, Inc. Austin TX). As discussed above, the regression equation was of the form:

$$\log(k_M) = \mathrm{a}\left(\frac{E_{SH}}{0.059}\right) + b\ \mathrm{pH} + c' \qquad [3.3]$$

Where k_M is the mass-normalized rate constant, E_{SH} is the reduction potential, and *a, b,* and *c'* are constants.

5. Results and Discussion

As in the previous sections, the project results and discussion are organized around the three main objectives of the project. For most of the figures in this section, the data used to construct the figures can be found in the appendices. (It should be noted that the order in which the results below are reported is not always chronological.)

5.A. Objective 1 – Demonstrate the utility of reactivity probes over a range of geochemical conditions

There are two primary components of this objective. The first was to evaluate possible reactivity probes for their applicability on field samples and the second was to examine reduction under iron- and sulfate-reducing conditions using our two laboratory columns.

We began this work by screening our proposed list of reactivity probes in controlled batch systems (Table 5.1.) The compounds were first tested for their stability in water in the rolling tube reactors. All of the compounds, with the exception of TCFE proved to be sufficiently stable for the expected duration of the experiments. Under control conditions the TCFE disappeared from solution at an observed rate of 0.0018/hour (Figure 5.1.), and as a result it was removed from the list.

Table 5. 1. Compounds tested for use as reactivity probes.

Compound	Abbreviation
Carbon Tetrachloride	CT
Trichloroethene	TCE
Trichlorofluoroethene	TCFE
Resazurin	Rzn
Resorufin	Rsf
Indigo Disulfonate	I2S
Indigo Tetrasulfonate	I4S

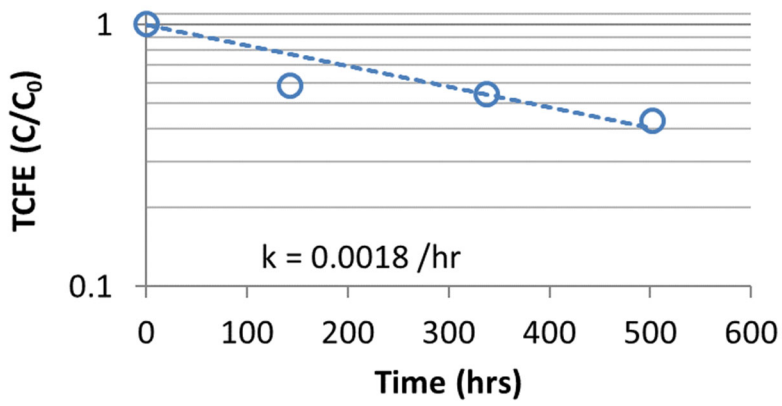

Figure 5.1. Example data for TCFE disappearance in control experiments. Concentration is normalized to the starting TCFE concentration for the experiment.

To evaluate the redox-active dyes, their rate of reduction was measured in batch tests using the RTRs and a subset of the field samples discussed under Objective 2.

The measured observed reduction rates for resazurin and indigo tetrasulfonate are plotted against measured reduction potential in Figure 5.2A. The dyes demonstrate a very binary rate behavior. This corresponds to the transition from just below to just above their standard reduction potentials. While this type of behavior is quite useful from the perspective of a redox indicator, it is not useful for estimating contaminant reduction rates.

The reduction rates of CT and TCE were also measured in these experiments (Figure 5.2 B and C). The relationships between reduction rate and E_{ES} for these cases were better behaved from the perspective of characterizing the rate.

To better understand the differences in behavior of these four compounds, it is useful to examine the standard reduction potentials for

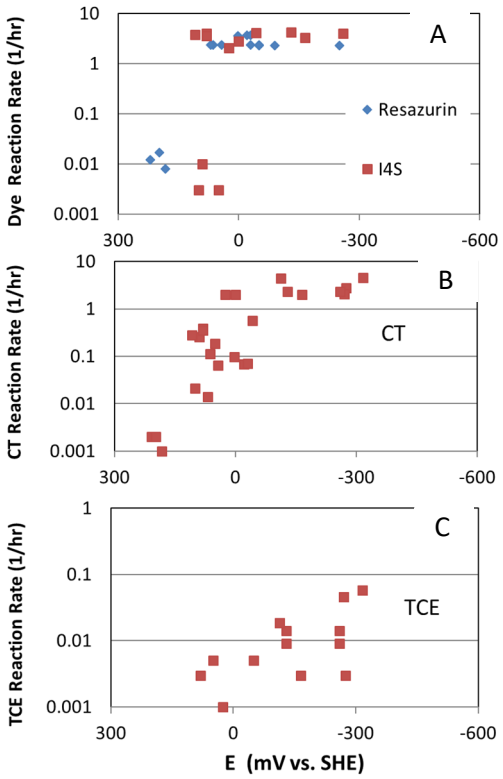

Figure 5. 2. Reduction rates for redox-active dyes. CT, and TCE as a function of measured reduction potential. The minimum measureable rate in these experiments is ~k=0.001/hr.

the dyes, CT and TCE. Figure 5.3. shows that the standard reduction potential for CT (~670mV), and TCE, ~540 mV) are well above expected reduction potentials for groundwater systems we examined (+250 to -350 mV vs. SHE). As a consequence, it is not surprising that the rates for CT and TCE increase consistently with decreasing potential, while the dyes transition sharply near their standard potentials.

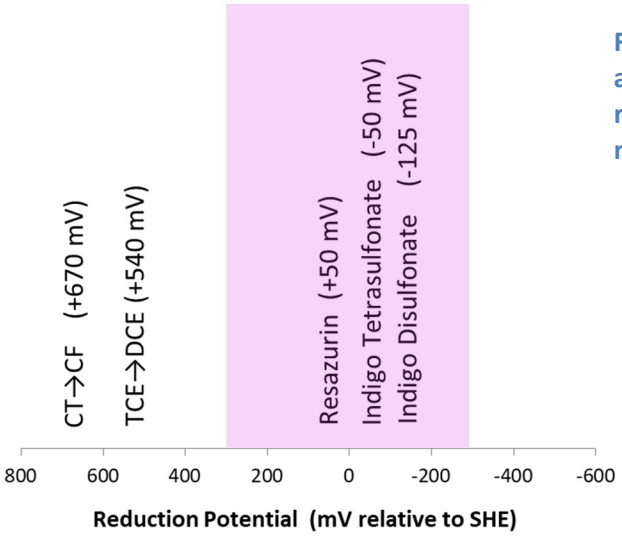

Figure 5. 3. Standard reduction potentials for CT, TCE and several redox-active dyes. Shaded purple area represents the range of reduction potential measured in field samples during this project

5.A.1. Measurement of TCE reduction rate in laboratory columns

Based on evaluation of the probes in the previous section, we selected CT and TCE for the reactivity experiments in the laboratory columns. The data in Figure 5.4. show TCE concentrations in the four column ports for each of the two laboratory columns (i.e., magnetite, M1, and magnetite+sulfate, S1) at the end of the injection phase of the experiments. The data indicate relatively rapid TCE reduction under flowing conditions. The times listed in the figure correspond to the approximate travel times down the column required to get to each port.

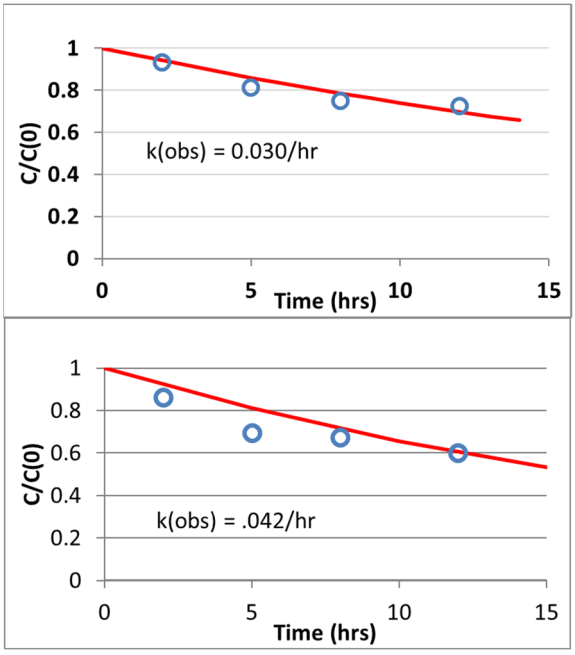

Figure 5. 4. TCE degradation down the magnetite (M1, upper) and magnetite+sulfate (S1, lower) columns. Concentrations are normalized to the influent concentrations in each case.

Once column flow was stopped, TCE concentrations and product formation were tracked at the first 3 sample ports. The elapsed time for each sampling event was adjusted by the initial travel time to reach that port (i.e., 200 hours after stopped flow, the time at port 2 would have been ~200+5 hours.) The data from all three ports are normalized to the concentration at the point in time when the flow was stopped and plotted as a function of time in Figure 5.5.

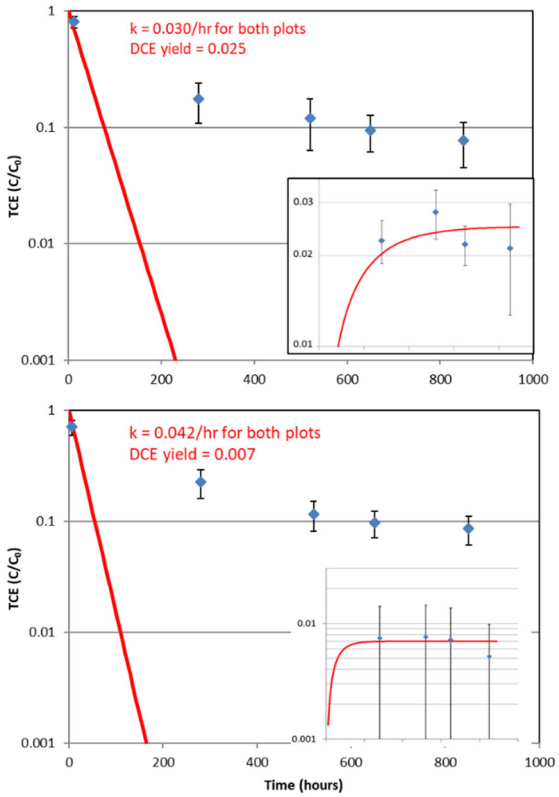

Figure 5. 5. TCE degradation (and DCE production) in the magnetite (upper) and sulfate (lower) columns during stopped flow.

The red line in each panel in Figure 5.5 represents the TCE concentration reduction that based on the rate determined under flowing conditions (Figure 5.4.). The data points (blue circles) for both columns indicate that the rate of TCE degradation decreased substantially from the rate observed during groundwater flow and continued to decrease over time (i.e., the slopes of the line segments decrease with time on this semi-log plot). The error bars represent +/-1 standard deviation of the normalized concentrations at the ports.

The inset figures in Figure 5.5 show DCE concentrations produced during the experiments. As the data indicate, the yield of DCE in these experiments was small, and it generally persisted through the experiment. All analyses were by GC/ECD, so only chlorinated products were detectable. No vinyl chloride was detected.

To better understand the loss of reactivity, the data in Figure 5.5 were fit with two models. Both are based on the second-order equation:

$$\frac{d[TCE]}{dt} = -k_{TCE}[TCE][SA] \qquad [5.1]$$

where $[SA]$ represents the surface area of the reactive phase. In Model 1, $[SA]$ is assumed to decrease stoichiometrically in proportion to the amount of TCE reduced

$$\frac{d[SA]}{dt} = -k_{TCE}[TCE][SA] \qquad [5.2]$$

In Model 2, the TCE degradation rate follows equation [5.1], but $[SA]$ also decreases by a first-order process that is independent of the TCE reduction rate

$$\frac{d[SA]}{dt} = -k_{TCE}[TCE][SA] - k_{SA}[SA] \qquad [5.3]$$

Figure 5.6. shows that both models fit the data reasonably well. As a consequence, it is difficult to determine which of them represents the more-accurate model.

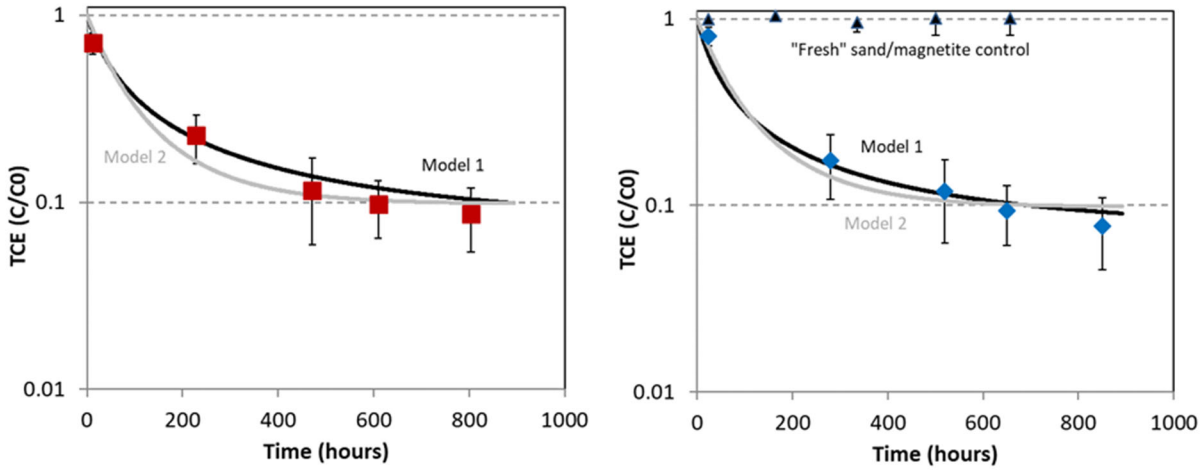

Figure 5. 6. TCE concentration data for column with sulfate (S1, red squares with 1 SD error bars) and without sulfate (M1, blue diamonds with 1 SD error bars) after flow was stopped in the columns.

To better compare the two models, the stopped-flow concentration data were used to estimate instantaneous mass-normalized rate constants for each time step. Those rates are compared to the overall rate constants derived from the two fitted models. As the data in Figure 5.7 indicate, the stoichiometrically-driven rate approach (Model 1) does a better job of fitting the data. It is also the most parsimonious model in that it requires only one rate constant, while model 2

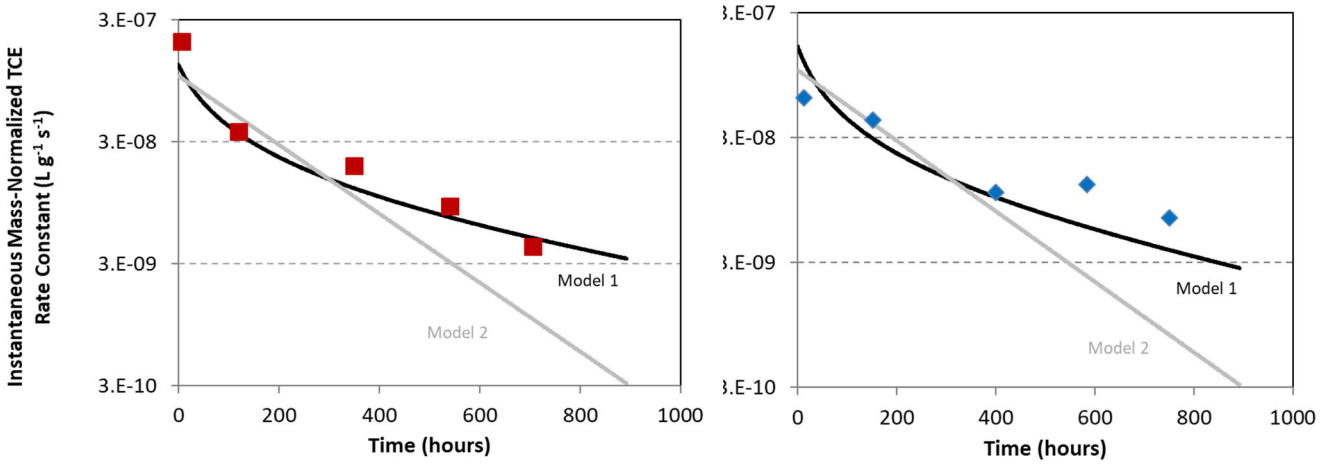

Figure 5. 7. Instantaneous mass-normalized rate constants estimated from the column data in Figure 3, and the two kinetic models (left=magnetite, right=magnetite+sulfate.

requires two.

5.A.2. Measurement of CT reduction rate in laboratory columns

Experimental conditions for the CT reduction experiments were similar to the TCE experiments. Unlike the TCE case, both columns showed significantly greater reactivity near the column influent (Figure 5.8.) For the magnetite column, this was primarily due to production of carbon monoxide. The CF production rate was relatively uniform down the column. For the sulfate column most of the CT reduction went to unknown non-chlorinated products, with some CS2 and CF production. Once again, however, CF production rate was relatively uniform down the column

Once flow was stopped in each column, samples were intermittently taken from each port and analyzed for CT and degradation products by GC/MS/FID to determine the starting conditions. Because of the high rate of CT degradation near the inlet of the columns, there were high background concentrations of some of the products at the start of the experiment. To better visualize the reactions, concentrations of CO, CF and CS2 at the beginning of the experiment were subtracted from the data such that net production at that location could be better assessed.

The background-subtracted data are shown in Figure 5.9. As indicated above, those data show CO production and CS2 production at Port 1 of the magnetite and sulfate columns, respectively. At ports 2 and 3 from both columns, CF was the only detected product

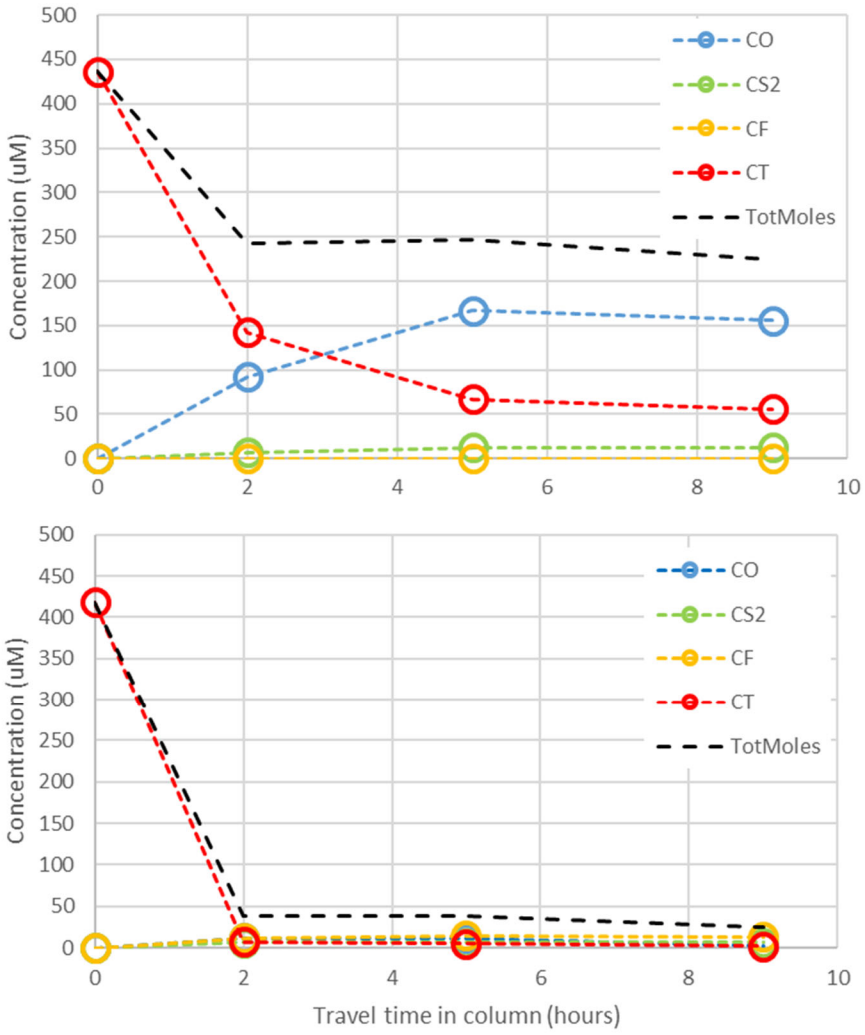

Figure 5. 8. . CT reduction and product formation at the sample ports during CT injection into the columns (upper=magnitite, lower=magnetite+sulfate)

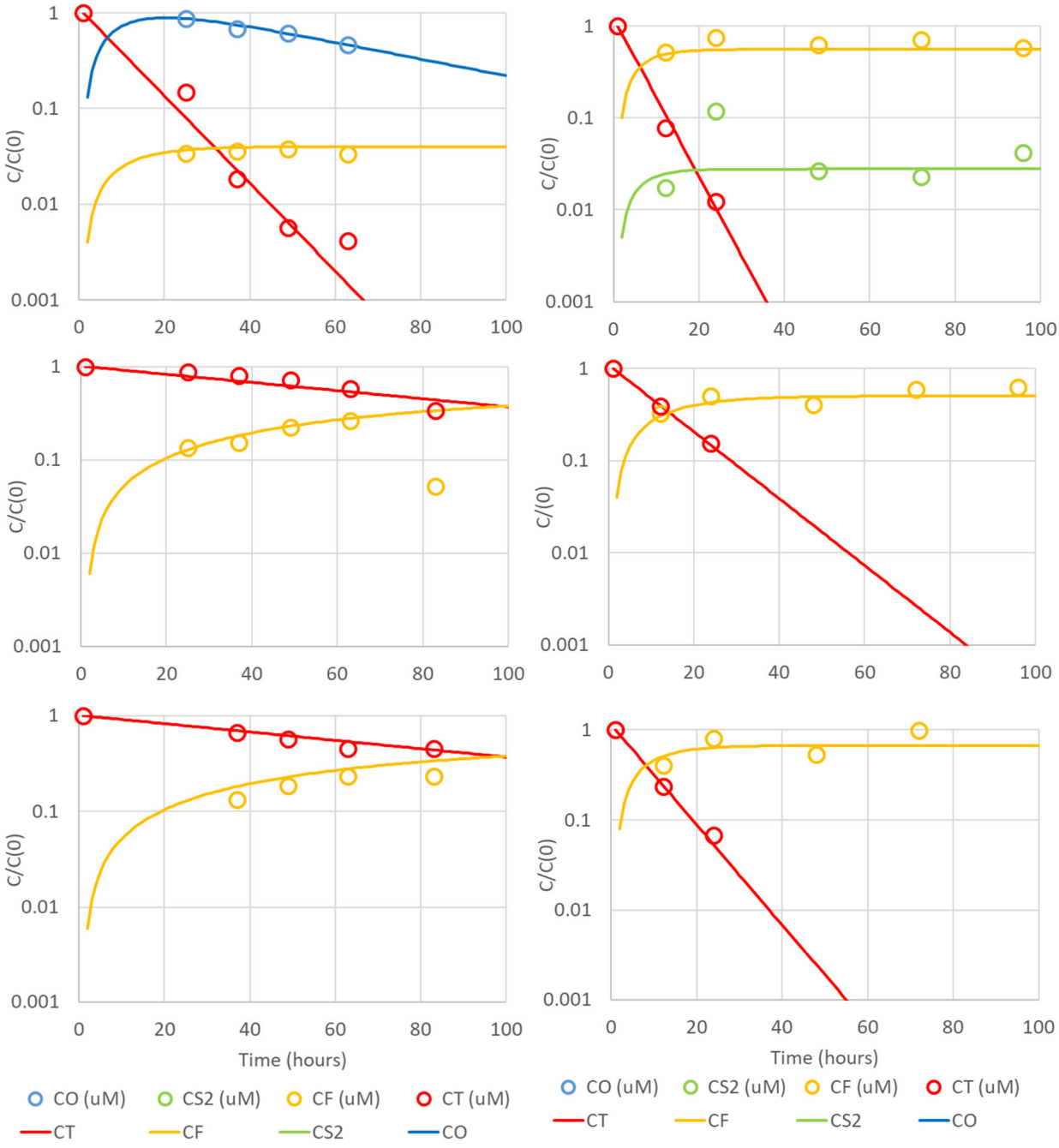

Figure 5. 9. CT reduction and product formation at the first 3 ports along the magnetite column (M1, left) and sulfate column (S1, right). Product concentrations reported here have had their "time=0" concentrations subtracted to better reflect production after column flow was stopped.

5.B. Objective 2. Measure abiotic reaction rates of actual field samples collected with the cryogenic core method

(Note: Some text and figures in this section were taken directly from our publication, Kocur et al., 2020)

5.B.1. Measurement of abiotic reaction rates on field samples

The CT disappearance and product formation data were fit to first-order rate constants (k_{OBS}) using a least-squares approach. Representative examples of the reaction data and first-order model fits are shown in the upper panels of Figure 5.10 – 5.13. In each of the examples in Figures 5.10-5.13, the modeled kinetic data were used to simulate the mass balance of detected products and are shown as the lower graphs in each figure.

It is important to note that CT degradation began immediately upon initiation of all of these experiments. Since none of these soils had been exposed to CT prior to the initiation, it can be safely concluded that the ability to degrade CT was present in the soils at the time the batch experiment was initiated. Further, because no carbon source was added to these batch experiments, no significant growth of a microbial population was expected. As a consequence, we conclude that in all these cases the degradation of CT was due to abiotic processes.

The patterns of product production in most of the samples in Figures 5.10-5.13 show some or significant production of CS2. This indicates that reduced sulfur-containing minerals (e.g., mackinawite) played a role in abiotic degradation. The notable exception to this for the cases examined was the SLOP site. Based on prior groundwater sampling at that site (Popovic et al., 2018), groundwater conditions were generally oxidizing, and sulfate concentrations persisted throughout the treatment zone as well as the background

The FEW data (Figure 5.12) are interesting in this context because sulfate concentrations are generally quite low at this site (Sale et al., 2016). However, ferrous iron concentrations are high, and the well is located down gradient from an old ZVI reactive barrier, so it could be that up-gradient conditions caused all of the naturally-occurring sulfate to be reduced and resulted in the widespread production of sulfide minerals.

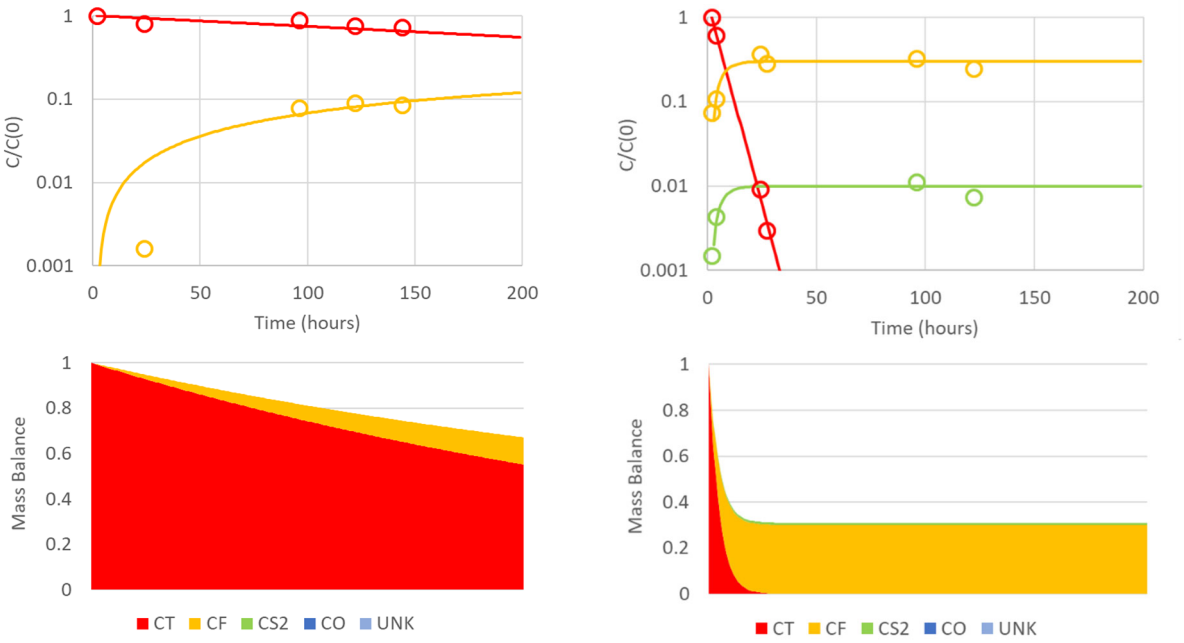

Figure 5. 10 . Example batch reactor data and modeled fits (upper graphs) and simulated mass balances (lower graphs) from the SLOP background (left) and SLOP treatment zone (right). Operational Unit 1.

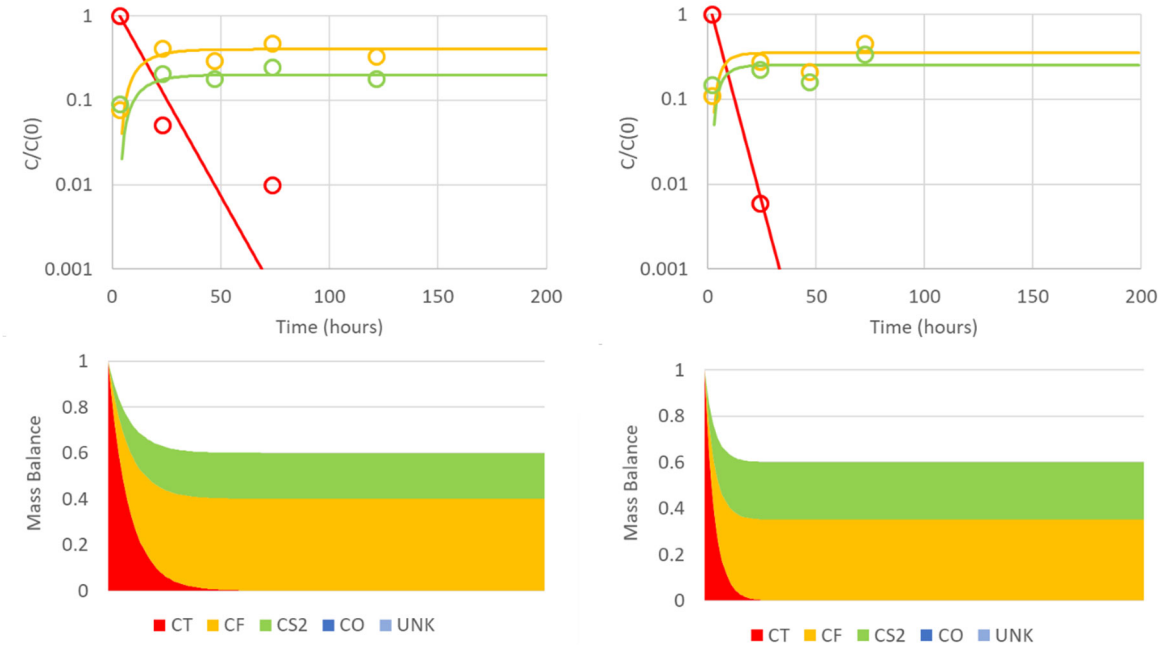

Figure 5. 11. Example batch reactor data and modeled fits (upper graphs) and simulated mass balances (lower graphs) from Parris Island MCRD Site 45.

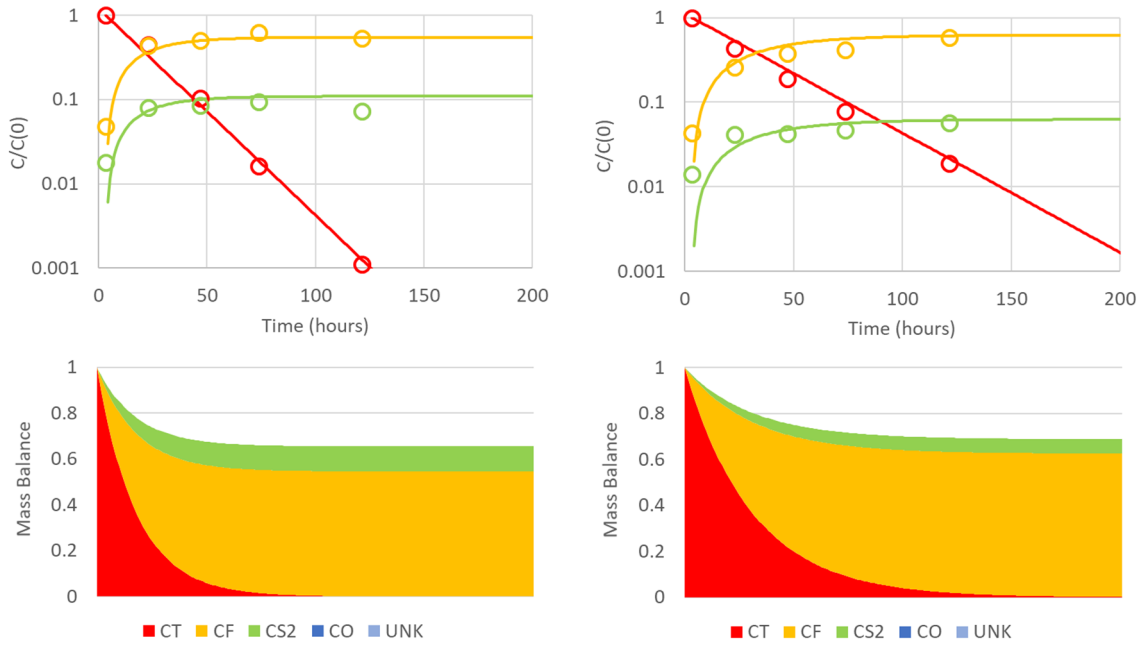

Figure 5. 12. Example batch reactor data and modeled fits (upper graphs) and simulated mass balances (lower graphs) from FE Warren AFB Spill Site 7 near MW 700.

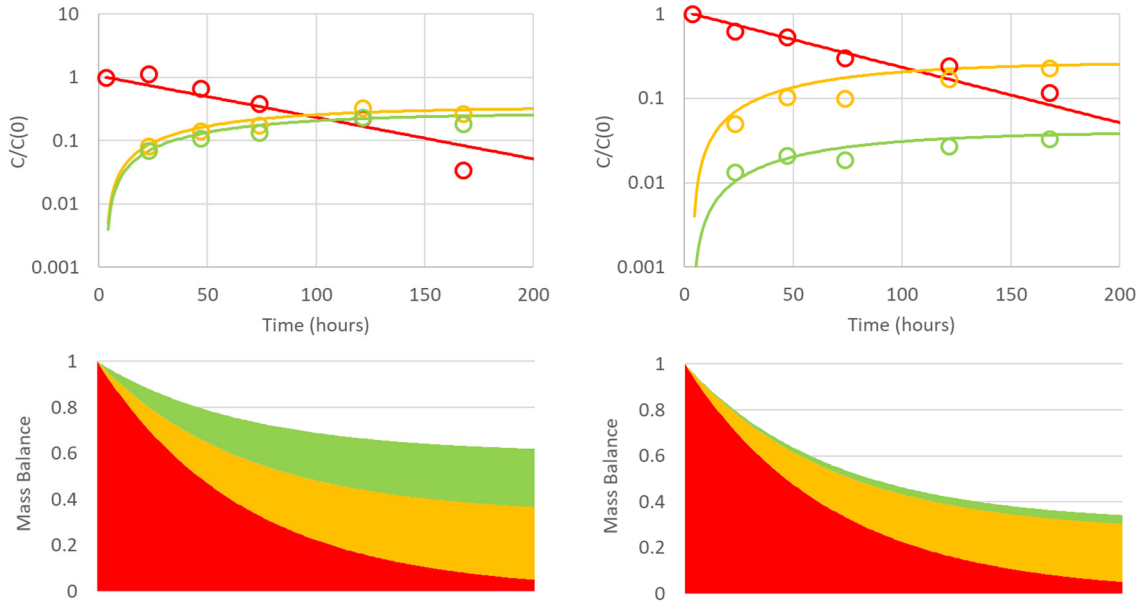

Figure 5. 13. Example batch reactor data and modeled fits (upper graphs) and simulated mass balances (lower graphs) from background sites at Indian Head NSWC, Site 17.

5.B.2. Correlation between Degradation Kinetics of CT and Reduction Potential

The rate constants observed in the RTR batch experiments were divided by their corresponding soil to water ratios to produce mass-normalized rate constants (k_M). The k_M values vary over 5 orders of magnitude, representing field condition-adjusted half-lives from a day to a decade, with treatment-zone locations generally exhibiting higher rates.

The electron shuttle-mediated reduction potential (E_{ES}) measurement data collected in the RTRs at the conclusion of each experiment are listed in Appendix C. This dual analysis allowed us to directly compare reactivity and reduction potential on each sample, and the data are shown in Figure 5.14. (pH was also measured and will be discussed in Objective 3.)

The data for each location show clear linear correlations between log(k_M) and mediated electrode potential (Figure 5.14). The statistical data for each location are listed in Table 5.2.

Site	Intercep	SD	Slope	SD	R^2	n
Indian Head NSWC	-3.31	0.039	-0.0075	0.00037	0.897	14
St. Louis Ordinance Plant OU1	-3.88	0.061	-0.0079	0.00044	0.954	6
Parris Island MCRD (TZ)	-3.2	0.035	-0.0089	0.0004	0.947	9
Parris Island MCRD (DG)	-1.98	0.202	-0.0091	0.00132	0.63	9
F.E. Warren AFB	-3.76	0.153	-0.0058	0.00074	0.835	5
All Data	-3.26	0.055	-0.0064	0.00041	0.595	43

Table 5. 2. Summary of regression parameters for log (km) vs E_{ES} data from the field sites. SD=standard deviation.

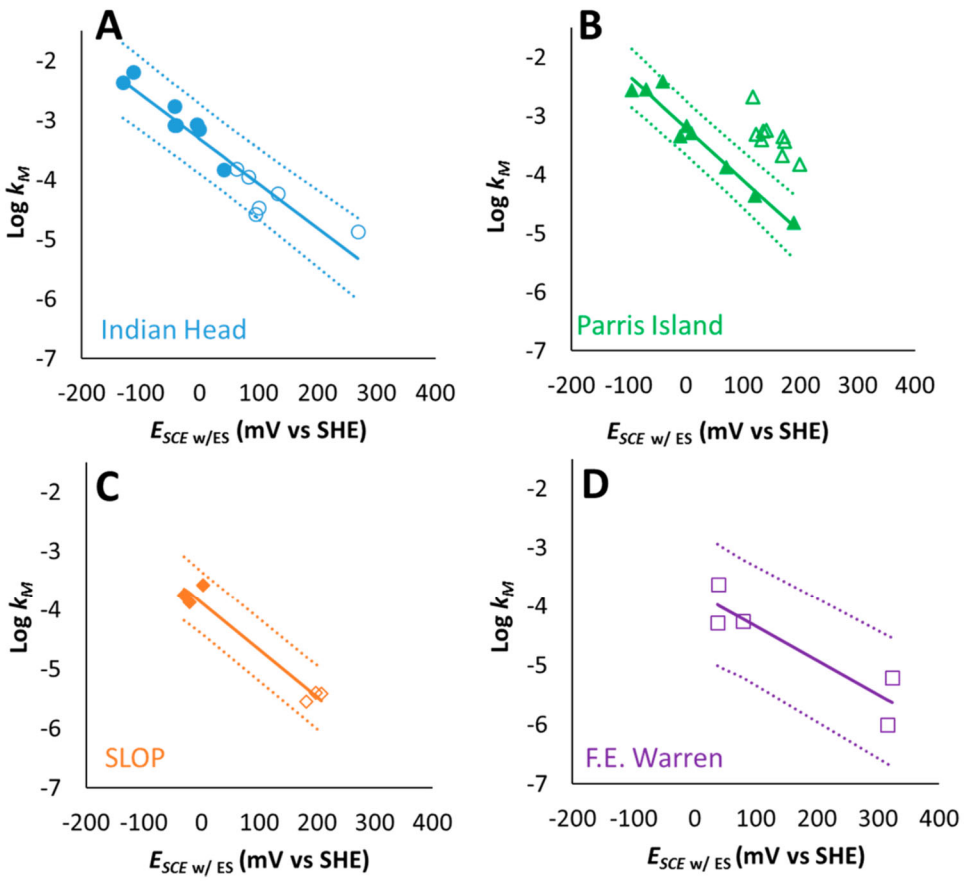

Figure 5. 14. Log k_M for CT degradation in RTRs vs mediated reduction potential measurement (ESCE w/ES) in the RTRs for four field sites showing site specific regression. This approach improves the confidence and predictive ability of mediated reduction potential, E_{ES} for four sites: (A) Indian Head, MD, (B) Parris Island, SC, (C) St. Louis Ordinance Plant (SLOP), MO, and (D) F. E. Warren Air Force Base, WY. Sample locations undergoing remediation (filled symbols) have notably higher rates and correspondingly lower potentials than background/downgradient (empty symbols) locations. Site specific regressions of log k_M fitting parameters against E_{ES} are shown (solid lines) with 95% confidence intervals (dotted lines). All samples were cryogenically preserved.

The data in Figure 5.14. were pooled and fit to one regression line (solid line in Figure 5.15) with the 95% prediction interval about the regression line. The data in Figure 5.15 demonstrate that appropriately measured reduction potentials on well-preserved aquifer solids can be predictive of contaminant degradation.

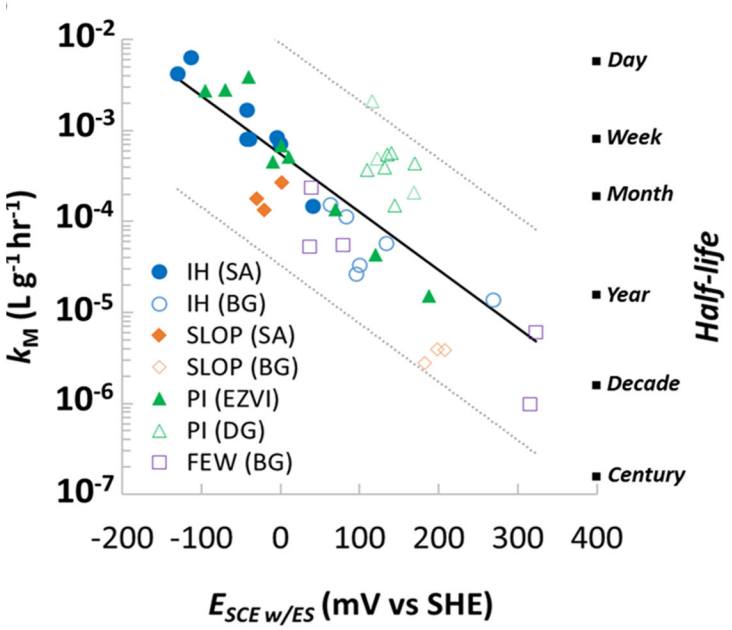

Figure 5. 15. Correlation between measured mass-normalized CT reduction rate constant and reduction potential for samples from four DoD sites.

There are a number of interesting aspect of this figure. The first is that the correlation is generally acceptable for all locations at all sites, despite differences in geochemistry at the sties. The second is that both source area and background sites show a similar relationship between log(k_M) and E. These data point not only to the validity of the fundamental relationship between reduction potential and rate, but also to the possibility that similar reactive mineral intermediates may control abiotic reactions at a wide range of site types.

Minimum Expected Reactivity. Given the uncertainties in site biogeochemistry and reactive surface area of individual field samples, the vertical scatter observed in Figure 5.15. may be difficult to reduce. However, the 95% prediction interval provides a basis for estimating the minimum expected reactivity based on a mediated electrode reduction potential measurement. For the data in Figure 5.15., the equation for the lower prediction interval (dotted line) is

$$\log(k_M) = -0.0148E_{ES} - 4.48 \quad [5.4]$$

These data suggest that a conservative reduction rate (95% confidence) can be estimated on the basis of a mediated electrode potential measurement.

5.B.3. Limitations of the Current Study.

There are several important caveats associated with Equation 5.4. The first is that it is calibrated only for carbon tetrachloride reduction. However, given the similarity of reaction mechanisms for CT and other important contaminants, it seems likely that equivalent correlations could be expected for other contaminants. A second caveat is that all of the RTR experiments were adjusted to circumneutral pH using carbonate buffer. Over the course of the experiments, many of the samples shifted in pH, presumably towards their native pH. Based on our data (Kocur et al 2020), the effect of pH might not be large. Alternately, as discussed under Objective 3, below, both pH and reduction potential can be factored into the correlation equation.

Other concerns regarding the general applicability of Equation 5.4. to predict reduction rates at field sites include the effect of freezing on reaction rates and reduction potential, as well as the effects of changing soil to water ratios, water chemistry, and mixing when making the laboratory measurements. The effects of freezing and storage are discuss under Objective 3, below. While additional experimental work is needed, these data demonstrate that high-quality soil cores and carefully measured reduction potentials can be predictive of measured reduction rates represents an important justification for continued research in this area. The demonstrated prediction of reduction rates for aquifer samples collected from contaminated sites using reduction potential measurements has clear practical importance and provides a new tool for assessing ANA. More careful inspection of individual site regressions, as in Figure 5.14., reveals that uncertainty can be greatly reduced using these measurement techniques on a site specific basis.

It should be noted that the regression is generally not useful when the redox conditions do not vary across a site. It should also be noted that uncertainty increases above a reduction potential of 0 mV versus SHE due to limitations of the selected electron shuttles. This limitation suggests there is a need to identify electron shuttles that are able to mediate potential measurements under mildly oxidizing conditions. Although Equation 5.4. is promising for screening level analysis, greater confidence can be drawn from this protocol when it is applied at a specific site.

5.C. Objective 3 - Determine if one or more of the RPs can provide robust measures of contaminant attenuation rates using cryogenically-collected core samples.

5.C.1. Prediction of reduction rate using reduction potential and pH

As discussed above, prediction of reduction rates for field samples is an important goal of this project. Using the data from Objective 2, including measured pH and reduction potential from the RTR batch experiments, we used multiple linear regression to fit the data to Equation 3.3.

$$\log(k_M) = \mathrm{a}\left(\frac{E}{0.059}\right) + b\ \mathrm{pH} + c' \qquad [3.3]$$

To accomplish this we developed a software program using Labview (NI, Inc. Austin TX). Figure 5.16 shows the front panel of this program. Built in functions within Labview allow multiple linear regression to be accomplished with a variety of algorithms. (The Labview virtual instrument is available from the investigators upon request.)

The resulting expression was

$$\log(k_M) = 0.178pH - 0.358\left(\frac{E_H}{0.059}\right) - 4.662 \qquad [5.5]$$

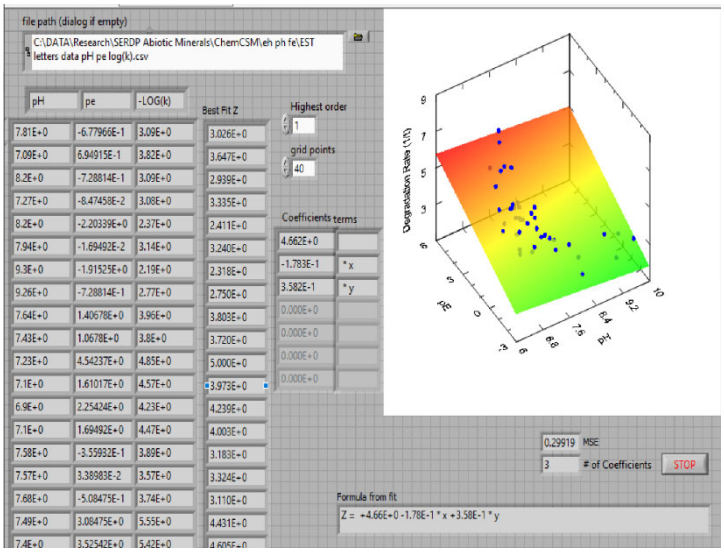

Figure 5. 16. Screen shot of the front panel of the Labview program used for multiple linear regression.

Using Equation 5.5 we can compare measured reaction rates to the model prediction. Generally this approach provided "within-an-order-of-magnitude" estimates of rate based on combined pH and reduction potential measurements (Figure 5.17).

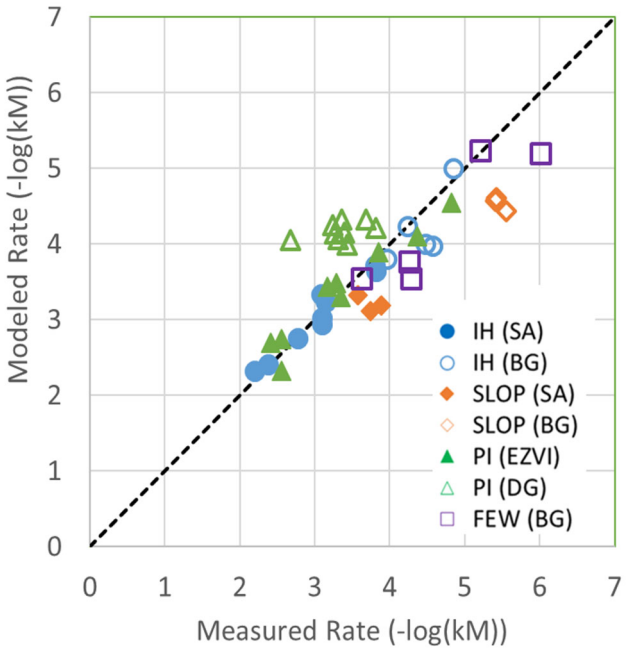

Figure 5. 17. Measured and modeled mass-normalized CT reduction rate constants for the field data collected as part of Objective 2.

5.C.2. Commonality of Reactive Phases across Sites.

As discussed above, the correlation of data from seven different locations at four different sites showed a very similar relationship between kM and EES, despite likely differences in (bio)geochemical conditions and SSAR. This suggests that there may be common processes controlling the reactive phases across the field sites. Abiotic rates are typically dictated by the biological activity in the system that is geochemically manifested as the availability of reduced phases. It is possible that the observed correlation is due to reactive mineral formation (precipitation) in situ and preserved in these samples. A number of reactive phases have been suggested on the basis of laboratory experiments [FeS, Fe(OH)2, and green rust].

The product formation data in Figures 5-10.-5.13 suggest that precipitated sulfur species (e.g., amorphous FeS) play an important role at most of the locations examined here. Since sulfate reduction is a very common occurrence at many contamination sites, we believe that those species likely represent important reactive phases. The precipitation of a single reactive mineral phase based on the bulk reduction potential in the system could explain the commonality between different field samples, leading to the relationship observed in this study. It is also likely that the reactive phase formation would increase as the mediated electrode potential decreases, leading to increased reactivity and the correlation between reduction potential and reduction rate.

5.C.3. Effects of freezing on reaction rates in batch experiments using column materials

While the predictive power of the data in the preceding sections is promising, it is important to examine the representativeness of the rates measured on core samples that have been frozen and stored. Samples from each of the laboratory columns discussed in Objective 1were used to evaluate the effects of freezing and storage. As discussed above, samples taken from well-mixed sections from both columns were tested for each of 3 sets of conditions (unfrozen, frozen, and frozen+stored). For each condition a set of sample triplicates was prepared and analyzed (i.e., 3 core sections * 3 sample conditions * 3 replicates * 2 columns = 54 individual experiments) using the RTRs.

Samples that were tested immediately after mixing of the column sections were labeled T0. Samples that were frozen and then tested the next day were labeled T1. Samples that were frozen and stored for 60 days were labeled T60. First order rate constants for CT disappearance, CF and CS2 appearance, and CO appearance and disappearance were determined for each experiment. To assess the effects of freezing, the rate constants from each individual experiment were divided by the rate constant from the corresponding unfrozen case (T0). These data were combined together to determine the average ratios for each reaction (e.g., for the kCT reaction, the ratios of the rates for all replicates from all ports were averaged). The data in Figure 5.18 indicate that the measured rates for the frozen and frozen+stored samples were generally at or above the levels observed in the unfrozen samples (i.e., average T1/T0 and T60/T0 values are greater than one). The CO production rate was an exception to this pattern. In addition, the measured rates for CO production were highly variable. We believe this is in large part due to the spatial variability of CO production and degradation within the columns. When we put these results in the context of the modeling work discussed above - where order-of-magnitude estimates are expected – our conclusion is that freezing and storage do not adversely impact measurement of reaction rates. We believe that this is an important conclusion of the work presented here.

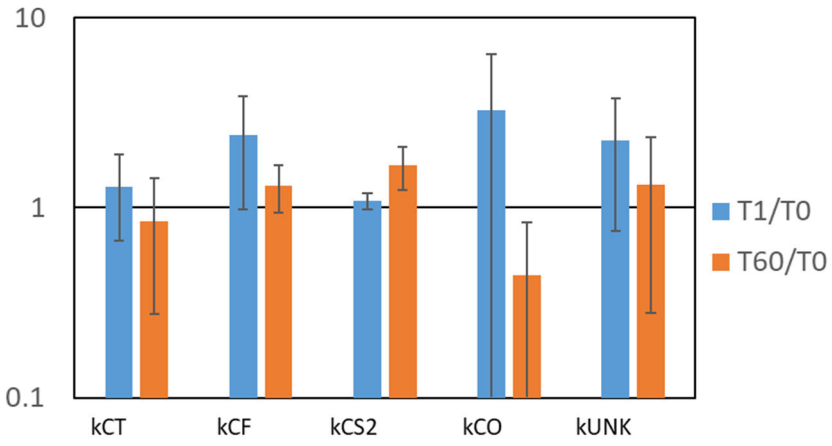

Figure 5. 18. Average ratios of frozen to unfrozen (T1/T0) and frozen+storage to unfrozen (T60/T0) for the two laboratory columns.

Comparison of field reactivity to pure mineral phases

Figure 5.19 compares data for one of the sites investigated in this study (Indian Head) to a previously reported kinetic correlation of carbon tetrachloride degradation and system potential for a 4 different minerals (Fan 2016). The figure shows that the Indian Head samples are more reactive than ferrous iron doped mineral, including freshly synthesized magnetite. This is somewhat surprising in that the bulk of the field sample mass is non-reactive materials. This supports the idea that the phases responsible for CT reduction in the field samples must be highly reactive. We believe this is primarily due to large surface areas of the in situ generated RMIs. For the Indian Head case, the CT reduction products (CS2 and CF, Figure 5.13) suggest that iron

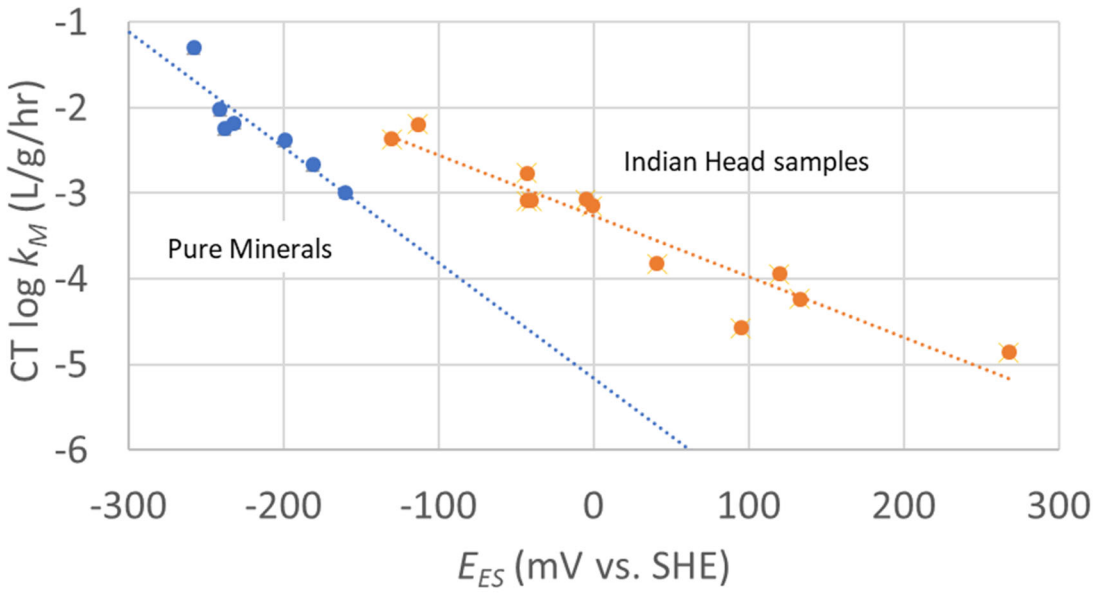

Figure 5. 19. Comparison of mass normalized rate constants for the Indian Head site (orange) samples to previously reported correlation for pure minerals (blue – Fan et al., 2016). Data for this figure can be found in Appendix C

sulfide was likely to have been an important reactive phase. These data serve as an example of how in situ produced minerals likely have a major impact on abiotic reactions in the subsurface.

6. Conclusions and Implications for Future Research/Implementation

We feel there are three primary benefits for DoD and for groundwater restoration in general from this work. These benefits align well with the three objectives of this research.

Objective 1 – Demonstrate the utility of reactivity probes over a range of geochemical conditions

We have demonstrated that CT works well as a reactivity probe for examining abiotic reduction. Reduction reaction rates are sufficiently rapid to make laboratory experiments practical. Based on our laboratory column experiments, the observed CT reduction reactions also produced products that may also be quite diagnostic (e.g., evidence for the role for reduced sulfur species).

Objective 2. Measure abiotic reaction rates of actual field samples collected with the cryogenic core method

The use of CT as a reactivity probe on core samples from field sites allows a rapid (i.e., within days) estimation of abiotic reduction rates. Those same samples allow accurate reduction potentials to be measured. By combining the measurement of reduction potential with CT reactivity probe measurements we have demonstrated that reduction rates can be predicted to within an order of magnitude of the measured value across a range of sites with a single regression equation. It is important to note here that the quality of the reduction potential measurement is key to this approach. Measurement using slurries of well-preserved core samples, along with an electron shuttle are critical to this success.

Reaction products for most of the field samples included a significant quantity of CS2 is produced. As indicated in Objective 1, and as has been reported previously, this is indicative of abiotic reduction by sulfur-containing minerals, and in particular amorphous iron sulfide. Furthermore, since most field sites have not been pre-exposed to CT, immediate reaction in batch experiments is a good indicator of abiotic reactions (i.e., no biological lag time was observed before degradation began).

Objective 3 - Determine if one or more reactiviey probes can provide robust measures of contaminant attenuation rates using cryogenically-collected core samples.

We have been able to further substantiate the utility of laboratory-based rate measurements by demonstrating that freezing and storage generally did not have a significant impact on measured reaction rates. As a consequence, we believe that the approach of cryogenic core collection followed by laboratory measurements (either kinetic experiments or measurement of E_{SH} and pH) provide viable approaches for prediction abiotic reactivity of aquifer materials

Implications for Future Research

The three conclusions above come with several suggestions for future research. First, the method should be demonstrated with other probes/contaminants in order to broaden the applicability of the approach. Second, the current approach should be applied on a broader range of field samples, again to broaden applicability. Finally, identification of the reactive phases that are active at field sites will be important in the context of insuring long-term abiotic reduction.

7. Literature Cited

Amonette, J. E.; Workman, D. J.; Kennedy, D. W.; Fruchter, J. S.; Gorby, Y. A., Dechlorination of carbon tetrachloride by Fe(II) associated with goethite. Environ. Sci. Technol. 2000, 34, 4606-4613.

Brow, C. N.; Johnson, R. O. B.; Xu, M.; Johnson, R. L.; Simon, H. M., Effects of cryogenic preservation and storage on the molecular characteristics of microorganisms in sediments. Environ. Sci. Technol. 2010, 44, (21), 8243-8247.

Brown, R. A.; Wilson, J. T.; Ferrey, M., Monitored natural attenuation forum: The case for abiotic MNA. Remediation J. 2007, 17, 127-137.

Butler, E. C.; Hayes, K. F., Kinetics of the transformation of trichloroethylene and tetrachloroethylene by iron sulfide. Environ. Sci. Technol. 1999, 33, 2021-2027.

Culpepper, J.; Scherer, M.; Robinson, T.; Neumann, A.; Cwiertny, D.; Latta, D., Reduction of PCE and TCE by magnetite revisited. Environ. Sci. Proc. Impacts 2018, 20, 1340-1349

Daneilsen, K.M. and K.F. Hayes, pH Dependence of Carbon Tetrachloride Reductive, Environ. Sci. Technol. 2004, 38, 4745-4752

Devlin, J.E. and D. Muller, Field and Laboratory Studies of Carbon Tetrachloride Transformation in a Sandy Aquifer under Sulfate Reducing Conditions, Environ. Sci. Technol. 1999, 33, 1021-1027

Elsner, M.; Haderlein, S. B.; Kellerhals, T.; Luzi, S.; Zwank, L.; Angst, W.; Schwarzenbach, R. P., Mechanisms and products of surface-mediated reductive dehalogenation of carbon tetrachloride by Fe(II) on goethite. Environ. Sci. Technol. 2004, 38, 2058-2066.

Fan, D.; Bradley, M.; Hinkle, A. W.; Johnson, R. L.; Tratnyek, P. G., Chemical reactivity probes for assessing abiotic natural attenuation by reducing iron minerals. Environ. Sci. Technol. 2016, 50, (4), 1868-1876.

Hageman, K., J.D. Istok, J.A. Field, T.E. Buscheck and L. Semprini, In Situ Anaerobic Transformation of Trichlorofluoroethene in Trichloroethene-Contaminanted Groundwater, Environ. Sci. Technol. 2001, 35, 1729-1735

He, Y. T.; Wilson, J. T.; Su, C.; Wilkin, R. T., Review of abiotic degradation of chlorinated solvents by reactive iron minerals in aquifers. Groundwater Monitoring & Remediation 2015, 35, 57-75.

Hyun, S.P. and K.F. Hayes, Feasibility of Using In Situ FeS Precipitation for TCE Degradation, J. Environ. Eng., 2009, 135(10): 1009-1014

Johnson, R. L.; Brow, C. N.; O'Brien Johnson, R.; Simon, H. M., Cryogenic Core Collection and Preservation of Subsurface Samples for Biomolecular Analysis. Ground Wat. Monitor. Remed. 2012, 33, 38-43.

Johnson, R.L. Cryogenic Collection of Complete Subsurface Samples for Molecular Biological Analysis, 2012, https://www.serdp-estcp.org/Program-Areas/Environmental-Restoration/Contaminated-Groundwater/Monitoring/ER-1559/(language)/eng-US

Kiaalhosseini, S.; Johnson, R. L.; Rogers, R. C.; Renno, M. I.; Lyverse, M.; Sale, T. C., Cryogenic core collection (C3) from unconsolidated subsurface media. Groundwater Monitoring & Remediation 2016, 36, 41-49.

Kenneke, J. F.; Weber, E. J., Reductive dehalogenation of halomethanes in iron- and sulfate-reducing sediments. 1. Reactivity pattern analysis. Environ. Sci. Technol. 2003, 37, 713-720.

Kiaalhosseini, S.; Johnson, R. L.; Rogers, R. C.; Renno, M. I.; Lyverse, M.; Sale, T. C., Cryogenic core collection (C3) from unconsolidated subsurface media. Groundwater Monitoring & Remediation 2016, 36, (4), 41-49.

Kocur, C. M. D.; Fan, D.; Tratnyek, P. G.; Johnson, R. L. Predicting abiotic reduction rates using cryogenically collected soil cores and mediated reduction potential measurements. *Environ. Sci. Technol. Lett.* 2020, 7, 1, 20–26

Lee, W.; Batchelor, B., Abiotic reductive dechlorination of chlorinated ethylenes by soil. Chemosphere 2004, 55, 705-713.

Macdonald, J. A., Evaluating natural attenuation for groundwater cleanup. Environ. Sci. Technol. 2000, 34, 346A-353A.

Mattes, T., Validation of Biotechnology for Quantifying the Abundance and Activity of Vinyl-chloride Oxidizers in Contaminated Groundwater ESTCP Project ER-201425, 2019

McCormick, M. L.; Adriaens, P., Carbon tetrachloride transformation on the surface of nanoscale biogenic magnetite particles. Environ. Sci. Technol. 2004, 38, 1045-1053.

Olson, M., Clayton, W.S., Sale, T., De Long, S.,Irianni-Renno, M., Johnson, R. Evaluating Long-Term Impacts of Soil-Mixing Source-Zone Treatment Using Cryogenic Core Collection; ESTCP: 2017.

Popovic, J.; Cook, L.; Wilkin, R. Analysis of Long-Term Performance of Zero-Valent Iron Applications; ESTCP: 2018.

Sale, T.; Olson, M.; Johnson, R. L.; Rogers, R. Third-Generation (3G) Site Characterization: Cryogenic Core Collection and High-Throughput Core Analysis - An Addendum to Basic Research Addressing Contaminants in Low Permeability Zones - A State of the Science Review, Final Report for SERDP Project ER-1740; 2016.

SERDP/ESTCP Summary Report: SERDP and ESTCP Workshop on Research and Development Needs for Chlorinated Solvents in Groundwater; 2018, https://www.serdp-estcp.org/News-and-Events/Conferences-Workshops/Past-ER-Workshops/Chlorinated-Solvents-Workshop-Report-2018.

SERDP, ERSON 2016-01, 2014, https://www.serdp-estcp.org/Funding-Opportunities/SERDP-Solicitations/Past-Solicitation-Pages/FY-2016-files/Core-SONs-FY16/ERSON-16-01

Shao, H. and E.C. Butler, Influence of Soil Minerals on the Rates and Products of Abiotic Transformation of Carbon Tetrachloride in Anaerobic Soils and Sediments, 2009, Environ. Sci. Technol., 45, 1896-1901

Shi, Z.; Nurmi, J. T.; Tratnyek, P. G., Effects of nano zero-valent iron (nZVI) on oxidation-reduction potential (ORP). Environ. Sci. Technol. 2011, 45, (5), 1586-1592.

Stewart, S. M.; Hofstetter, T. B.; Joshi, P.; Gorski, C. A., Linking thermodynamics to pollutant reduction kinetics by Fe2+ bound to iron oxides. Environ. Sci. Technol. 2018, 52, (10), 5600-5609.

Stewart, S. M.; Hofstetter, T. B.; Joshi, P.; Gorski, C. A., Linking thermodynamics to pollutant reduction kinetics by Fe2+ bound to iron oxides. Environ. Sci. Technol. 2018, 52, 5600-5609.

Tratnyek, P.G. and R.L. Johnson, Practical Assessment and Optimization of Redox-Based Groundwater Remediation Technologies, 2017, SERDP ER-2308. https://www.serdp-estcp.org/Program-Areas/Environmental-Restoration/Contaminated-Groundwater/Persistent-Contamination/ER-2308/ER-2308-FR/(modified)/09May2017

U.S. EPA (2009) Identification and Characterization Methods for Reactive Minerals Responsible for Natural Attenuation of Chlorinated Organic Compounds in Ground Water, EPA 600/R-09/115

Vancheeswaran, S., M.R. Hyman, and L. Semprini, Anaerobic Biotransformation of Trichlorofluoroethene in Groundwater Microcosms, Environ. Sci. Technol. 1999, 33, 2040-2045

Wilkin, R.T. Mineralogical Preservation of Solid Samples Collected from Anoxic Subsurface Environments, 2006, EPA/600/R-06/112.

8. Appendices

Appendix A. Data used in Section 5 Figures

Figure 5.1. Normalized TCFE concentration in the control experiment

Time (h)	TCFE C/C(0)
0.00	1.00
142.35	0.59
336.85	0.55
502.00	0.43

Figure 5.2.

Samples	Rsn Rate	I4S	CT Rate Constant	TCE Rate Constant
	1/hr	1/hr	1/hr	1/hr
SLOP 001 A5	3.7		0.068	0.0001
SLOP 001 B5	3.6		0.098	0.0001
SLOP 001 C5	3.7		0.071	0.0001
SLOP 003 A5	0.008		0.001	0.0001
SLOP 003 B5	0.012		0.002	0.0001
SLOP 003 C5	0.017		0.002	0.0001
E104	2.32		2.0483	0.046
E105	2.33		4.5171	0.0573
E109	2.34		4.4328	0.0185
E97		4.14	0.569	
E99		4.28	2.3	0.014
E103		3.95	2.3	0.009
E121	2.35		0.0647	0.0001
E128	2.36		0.1123	0.0001
E133	2.37		0.0141	0.0001
E135		0.003	0.187	0.005
E140		0.01	0.259	
E149		0.003	0.021	0.0001
PI-03-11		3.768189188	0.28	0.0001
P1-03-17		3.967788377	0.381	0.0001
PI-04-05		3.552250539	0.348	0.003
PI-06-05		2.818205222	2	0.0004
PI-06-11		2.02908443	2	0.001
PI-06-17		3.265830821	2	0.003

Figure 5.4

M1 Column		S1 Column	
Time (hrs)	TCE C/C(0)	Time (hrs)	TCE C/C(0)
12	0.7268	12	0.6024
8	0.7502	8	0.6742
5	0.8120	5	0.6948
2	0.9328	2	0.8624

Figure 5.5 to 5.7

		Normalized Conc.		
	Time (hrs)	DCE	TCE	
	12	0.0000	0.7268	
	8	0.0000	0.7502	
	5	0.0000	0.8120	
	2	0.0000	0.9328	
	288	0.0242	0.1140	
	282	0.0227	0.1397	
	276	0.0256	0.1772	
	270	0.0173	0.2644	
	531	0.0245	0.0505	
	525	0.0304	0.1036	
	519	0.0338	0.1382	
	513	0.0226	0.1844	
	663	0.0241	0.0723	
	657	0.0232	0.0778	
	651	0.0181	0.1322	
	856	0.0307	0.0712	
	850	0.0177	0.0486	
	844	0.0150	0.1122	
	Avg(TCE)	Stdev(TCE)	Avg(DCE)	Stdev(DCE)
12	0.8054	0.0922	0.0000	0.0000
280	0.1738	0.0657	0.0224	0.0037
520	0.1192	0.0565	0.0278	0.0052
650	0.0941	0.0331	0.0218	0.0032

Figure 5.5 to 5.7 (cont.)

		Normalized Conc.		
Port	Time (hrs)	DCE	TCE	
4	12	0.0000	0.6024	
3	8	0.0000	0.6742	
2	5	0.0000	0.6948	
1	2	0.0000	0.8624	
4				
3	234	0.0000	0.2076	
2	228	0.0103	0.1718	
1	222	0.0121	0.3007	
4				
3	477	0.0000	0.0977	
2	471	0.0102	0.0938	
1	465	0.0126	0.1565	
3	616	0.0000	0.0815	
2	610	0.0123	0.0833	
1	604	0.0094	0.1267	
3	810	0.0000	0.0702	
2	804	0.0067	0.0736	
1	798	0.0089	0.1158	
Time (hrs)	Avg(TCE)	Stdev(TCE)	Avg(DCE)	Stdev(DCE)
6	0.7084	0.1100	0.0000	0.0000
280	0.2267	0.0665	0.0075	0.0065
520	0.1160	0.0352	0.0076	0.0067
650	0.0972	0.0256	0.0072	0.0064
850	0.0865	0.0254	0.0052	0.0046

Figure 5.8.

Time (hrs)	CO (uM)	CS2 (uM)	CF (uM)	CT (uM)	TotMoles
0	0.01	0.01	0.01	436.00	436.03
2	92.39	0.00	7.04	142.64	242.07
5	166.86	0.00	12.54	66.71	246.11
9	155.63	0.00	12.82	55.55	224.01

Time (hrs)	CO (uM)	CS2 (uM)	CF (uM)	CT (uM)	TotMoles
0	0.01	0.01	0.01	418.00	418.03
2	12.19	6.66	12.01	7.45	38.31
5	12.00	6.98	15.12	4.86	38.97
9	2.60	6.42	13.60	1.98	24.60

Figure 5.9.

M-COL-STOP-P1						S-COL-STOP-P1				
1.500	0.400					1.500	0.400			
Time	CO (uM)	CS2 (uM)	CF (uM)	CT (uM)		Time	CO (uM)	CS2 (uM)	CF (uM)	CT (uM)
1.000	0.000	0.000	0.000	1.000		1.000	0.000	0.000	0.000	1.000
25.000	0.870	0.000	0.034	0.148		12.250	0.000	0.017	0.523	0.078
37.000	0.676	0.000	0.036	0.018		24.000		0.118	0.743	0.012
49.000	0.614	0.000	0.038	0.006		48.000		0.027	0.621	0.000
63.000	0.460	0.000	0.033	0.004		72.000		0.023	0.705	0.000
						96.000		0.042	0.581	0.000
M-COL-STOP-P2						S-COL-STOP-P2				
1.500	0.400					1.500	0.400			
Time	CO (uM)	CS2 (uM)	CF (uM)	CT (uM)		Time	CO (uM)	CS2 (uM)	CF (uM)	CT (uM)
1	0.000	0.000	0.000	1.000		1	0.000	0.000	0.000	1.000
25	0.000	0.000	0.135	0.869		12	0.000	0.000	0.323	0.387
37	0.000	0.000	0.154	0.800		24	0.000	0.000	0.501	0.153
49	0.000	0.000	0.221	0.713		48	0.000	0.000	0.404	0.000
63	0.000	0.000	0.262	0.577		72	0.000	0.000	0.590	0.000
83	0.000	0.000	0.052	0.336		96	0.000	0.000	0.617	0.000
M-COL-STOP-P3						S-COL-STOP-P2				
1.500	0.400					1.500	0.400			
Time	CO (uM)	CS2 (uM)	CF (uM)	CT (uM)		Time	CO (uM)	CS2 (uM)	CF (uM)	CT (uM)
1	0.000	0.000	0.000	1.000		1	0.000	0.000	0.000	1.000
37	0.000	0.000	0.133	0.670		12	0.000	0.000	0.323	0.387
49	0.000	0.000	0.187	0.573		24	0.000	0.000	0.501	0.153
63	0.000	0.000	0.234	0.456		48	0.000	0.000	0.404	0.000
83	0.000	0.000	0.234	0.456		72	0.000	0.000	0.590	0.000
						96	0.000	0.000	0.617	0.000

Figure 5.10 to 5.13.

MIX-CT3-05-SLOP-03				
20	60			
Time (hrs)	[CO] (uM)	[CS2] (uM)	[CF] (uM)	[CT] (uM)
2	0	0	0	1
24	0	0	0.001607	0.810172
96	0	0	0.078136	0.878852
122	0	0	0.090838	0.759655
144	0	0	0.085331	0.726001

MIX-CT3-04-SLOP-01				
20	60			
Time (hrs)	[CO] (uM)	[CS2] (uM)	[CF] (uM)	[CT] (uM)
2	0	0.001503	0.074058	1
4	0	0.00437	0.10773	0.60665
24	0	0	0.365548	0.009177
27	0	0	0.281388	0.002951
96	0	0.011104	0.321786	0
122	0	0.00742	0.2452	0

MIX-CT2-03-PI-13-5				
20	60			
Time (hrs)	[CO] (uM)	[CS2] (uM)	[CF] (uM)	[CT] (uM)
2	0	0.146666	0.109974	1
24	0	0.225176	0.27508	0.005933
47	0	0.15959	0.211627	0
72.5	0	0.338303	0.457484	0

Figure 5.10 to 5.13. (cont)

MIX-CT1-06-PI-27-11				
20	60			
Time (hrs)	[CO] (uM)	[CS2] (uM)	[CF] (uM)	[CT] (uM)
3.4	0	0.090951	0.076556	1
23	0	0.205131	0.413866	0.050966
47	0	0.181213	0.293717	0
73.75	0	0.245353	0.471506	0.009992
121.5	0	0.179762	0.329255	0

MIX-CT1-05-FEW-9-16				
20	60			
Time (hrs)	[CO] (uM)	[CS2] (uM)	[CF] (uM)	[CT] (uM)
3.4	0	0.018039	0.048346	1
23	0	0.079645	0.438433	0.445981
47	0	0.084541	0.501793	0.104416
73.75	0	0.093719	0.624726	0.016091
121.5	0	0.072507	0.527996	0.0011

IX-CT1-04-FEW-9-10				
20	60			
Time (hrs)	[CO] (uM)	[CS2] (uM)	[CF] (uM)	[CT] (uM)
3.4	0	0.014072	0.043267	1
23	0	0.041408	0.257403	0.437328
47	0	0.042565	0.37722	0.190664
73.75	0	0.046473	0.420426	0.078414
121.5	0	0.056713	0.57744	0.018776

Figure 5.10 to 5.13. (cont)

MIX-CT1-03-E140				
20	60			
Time (hrs)	[CO] (uM)	[CS2] (uM)	[CF] (uM)	[CT] (uM)
3.4	0	0	0	1
23	0	0.068878	0.080638	1.119483
47	0	0.108839	0.140026	0.667063
73.75	0	0.133483	0.174006	0.388193
121.5	0	0.230608	0.327991	0.229165
167.5	0	0.185799	0.264522	0.03405

MIX-CT1-02-E135				
20	60			
Time (hrs)	[CO] (uM)	[CS2] (uM)	[CF] (uM)	[CT] (uM)
3.4	0	0	0	1
23	0	0.013397	0.049487	0.618981
47	0	0.021011	0.104132	0.529881
73.75	0	0.018519	0.098893	0.302931
121.5	0	0.027071	0.169539	0.24191
167.5	0	0.033289	0.22783	0.116328

Figures 5.14 and 5.15.

Sample ID	Borehole	Fe^{2+} (mg/L)	pH	$E_{SCE\ /\ ES}$ (mV vs SHE)	k_M (L/g/hr)
IH-SA2-3.79-93	SA2	4.20E-01	7.81	-40	8.20E-04
IH-SA2-4.29-92	SA2	1.20E+00	7.09	41	1.50E-04
IH-SA2-9.29-97	SA2	1.10E+00	8.2	-43	8.20E-04
IH-SA2-11.21-101	SA2	6.90E-01	7.27	-5	8.40E-04
IH-SA2-11.79-99	SA2	7.10E-02	8.2	-130	4.30E-03
IH-SA2-14.21-102	SA2	3.70E-02	7.94	-1	7.20E-04
IH-SA2-18.79-109	SA2	1.00E-02	9.3	-113	6.40E-03
IH-SA2-19.29-108	SA2	9.80E-03	9.26	-43	1.70E-03
IH-DG2B-14.29-121	DG2B	2.30E-01	7.64	83	1.10E-04
IH-DG2B-15.29-128	DG2B	ND	7.43	63	1.60E-04
IH-DG2B-17.79-133	DG2B	2.80E-01	7.23	268	1.40E-05
IH-DG2A-4.29-135	DG2A	7.90E-01	7.1	95	2.70E-05
IH-DG2A-9.29-140	DG2A	8.00E-01	6.9	133	5.90E-05
IH-DG2A-14.29-149	DG2A	ND	7.1	100	3.40E-05
SLOP-SB001-1618-A6	SB001	9.60E-03	7.58	-21	1.30E-04
SLOP-SB001-1618-B6	SB001	1.80E-02	7.57	2	2.70E-04
SLOP-SB001-1618-C6	SB001	9.30E-03	7.68	-30	1.80E-04
SLOP-SB003-1618-A6	SB003	1.70E-02	7.49	182	2.80E-06
SLOP-SB003-1618-B6	SB003	5.80E-02	7.4	208	3.80E-06
SLOP-SB003-1618-C6	SB003	7.70E-02	7.24	198	3.90E-06
PI-03-11	Borehole 1	1.10E+01	7.31	-10	4.50E-04
P1-03-17	Borehole 1	2.90E+01	6.93	1	6.80E-04
PI-04-05	Borehole 1	4.10E-01	6.96	10	5.10E-04
PI-06-05	Borehole 1	2.60E-02	9.9	-95	2.80E-03
PI-06-11	Borehole 1	ND	9.69	-40	3.90E-03
PI-06-17	Borehole 1	2.70E-02	8.36	-70	2.80E-03

PI-04-11	Borehole 1	ND	7.25	120	4.30E-05
PI-04-17	Borehole 1	2.40E+00	7.05	188	1.50E-05
PI-05-05	Borehole 1	2.40E-01	6.73	70	1.40E-04
PI-13-05	Borehole 2	2.10E-02	7.51	110	3.70E-04
PI-13-11	Borehole 2	ND	7.09	140	5.70E-04
PI-13-17	Borehole 2	ND	7.67	170	4.40E-04
PI 20-5	Borehole 3	ND	7.61	168	2.10E-04
PI 20-11	Borehole 3	ND	7.35	116	2.10E-03
PI 20-17	Borehole 3	ND	7.5	122	4.90E-04
PI 26-23	Borehole 4	2.10E-02	7.51	135	5.50E-04
PI 27-5	Borehole 4	2.30E-02	7.4	132	4.00E-04
PI 27-11	Borehole 4	2.20E-02	7.4	144	1.50E-04
FEW 9-10	MW700A	2.40E-01	7.54	37	5.30E-05
FEW 9-16	MW700A	1.30E-01	7.72	79	5.50E-05
FEW 9-21	MW700A	NA	7.6	39	2.40E-04
FEW 10-4	MW700A	6.80E-01	7.71	315	9.80E-07
FEW 10-10	MW700A	6.90E-01	7.76	323	6.10E-06

Figure 5.17.

Sample	Boring	-log(kM) measured	-log(kM) modeled
IH-SA2-3.79-93	**SA2**	3.09	3.026
IH-SA2-4.29-92	SA2	3.82	3.647
IH-SA2-9.29-97	SA2	3.09	2.939
IH-SA2-11.21-101	SA2	3.08	3.335
IH-SA2-11.79-99	SA2	2.37	2.411
IH-SA2-14.21-102	SA2	3.14	3.24
IH-SA2-18.79-109	SA2	2.19	2.318
IH-SA2-19.29-108	SA2	2.77	2.75
IH-DG2B-14.29-121	DG2B	3.96	3.803
IH-DG2B-15.29-128	DG2B	3.8	3.72
IH-DG2B-17.79-133	DG2B	4.85	5
IH-DG2A-4.29-135	DG2A	4.57	3.973
IH-DG2A-9.29-140	DG2A	4.23	4.239
IH-DG2A-14.29-149	DG2A	4.47	4.003
SLOP-SB001-1618-A6	SB001	3.89	3.183
SLOP-SB001-1618-B6	SB001	3.57	3.324
SLOP-SB001-1618-C6	SB001	3.74	3.11
SLOP-SB003-1618-A6	SB003	5.55	4.431
SLOP-SB003-1618-B6	SB003	5.42	4.605
SLOP-SB003-1618-C6	SB003	5.41	4.573
PI-03-11	Borehole 1	3.35	3.298
P1-03-17	Borehole 1	3.17	3.432
PI-04-05	Borehole 1	3.29	3.482
PI-06-05	Borehole 1	2.55	2.32
PI-06-11	Borehole 1	2.41	2.691
PI-06-17	Borehole 1	2.55	2.746
PI-04-11	Borehole 1	4.37	4.098
PI-04-17	Borehole 1	4.82	4.546
PI-05-05	Borehole 1	3.85	3.887
PI-13-05	Borehole 2	3.43	3.991
PI-13-11	Borehole 2	3.24	4.248
PI-13-17	Borehole 2	3.36	4.326
PI 20-5	Borehole 3	3.68	4.325
PI 20-11	Borehole 3	2.68	4.056

PI 20-17	Borehole 3	3.31	4.065
PI 26-23	Borehole 4	3.26	4.142
PI 27-5	Borehole 4	3.4	4.144
PI 27-11	Borehole 4	3.82	4.217
FEW 9-10	MW700A	4.28	3.542
FEW 9-16	MW700A	4.26	3.765
FEW 9-21	MW700A	3.62	3.543
FEW 10-4	MW700A	6.01	5.199
FEW 10-10	MW700A	5.21	5.239

Figure 5.18.

			kCT	kCF	kCS2	kCO	kUNK
M1	Port 1	T1/T0	2.017779	2.410538		1.53895	3.673796
		T60/T0	0.747306	0.829795		0.151323	0.532707
	Port 2	T1/T0	0.485192	5.198444		7.094004	2.389623
		T60/T0	0.079263	1.304222		0.892281	2.491666
	Port 3	T1/T0	0.853198	2.168312		1.150313	0.691347
		T60/T0	0.513536	1.615499		0.286556	0.92384
S1	Port 1	T1/T0	1.054518	1.299972	1.130995		
		T60/T0	0.920191	1.243709	1.338268		
	Port 2	T1/T0	1.362415	1.261466	1.158246		
		T60/T0	1.06119	1.011988	1.505637		
	Port 3	T1/T0	1.991904	2.194882	0.968048		
		T60/T0	1.803488	1.803122	2.158006		
	All Ports	Avg(T1/T0)	1.294168	2.422269	1.085763	3.261089	2.251589
		Avg(T60/T0)	0.854162	1.301389	1.667304	0.443387	1.316071
		Stdev(T1/T0)	0.619909	1.444334	0.102851	3.2	1.496008
		Stdev(T60/T0)	0.579026	0.363288	0.433122	0.39459	1.036709

Figure 5.19

Sample	Fe 2+ loading (mmol/g)	ECRP (mV vs SHE)	Log *kM*
Goethite	0.166666667	-232	-2.18
Goethite	0.333333333	-241	-2.02
Goethite	0.1	-181	-2.67
Lepidocrocite	0.37037037	-199	-2.38
Lepidocrocite	0.1	-160	-2.99
Magnetite	0	-238	-2.25
Magnetite	0.333333333	-258	-1.3

Sample	E (w/ ES) (mV vs SHE)	Log (*kM*)
IH - SA2 - 3.79 - 93	-40	-3.088
IH - SA2 - 4.29 - 92	41	-3.826
IH - SA2 - 9.29 - 97	-43	-3.086
IH - SA2 - 11.21 - 101	-5	-3.073
IH - SA2 - 11.79 - 99	-130	-2.369
IH - SA2 - 14.21 - 102	-1	-3.146
IH - SA2 - 18.79 - 109	-113	-2.193
IH - SA2 - 19.29 - 108	-43	-2.766
IH - DG2B - 14.29 - 121 b	120	-3.944
IH - DG2B - 17.79 - 133 b	268	-4.861
IH - DG2A - 4.29 - 135 b	95	-4.571
IH - DG2A - 9.29 - 140 b	133	-4.232

Appendix B. Publications

Kocur, C. M. D.; Fan, D.; Tratnyek, P. G.; Johnson, R. L. Predicting abiotic reduction rates using cryogenically collected soil cores and mediated reduction potential measurements. *Environ. Sci. Technol. Lett.* 2020, 7, 1, 20–26